



HAL
open science

Engineering Novel 3D Models to Recreate High-Grade Osteosarcoma and its Immune and Extracellular Matrix Microenvironment

Marina Pierrevelcin, Vincent Flacher, Christopher G Mueller, Romain Vauchelles, Eric Guerin, Benoît Lhermitte, Erwan Pencreach, Andreas Reisch, Quentin Muller, Loyal Doumard, et al.

► To cite this version:

Marina Pierrevelcin, Vincent Flacher, Christopher G Mueller, Romain Vauchelles, Eric Guerin, et al.. Engineering Novel 3D Models to Recreate High-Grade Osteosarcoma and its Immune and Extracellular Matrix Microenvironment. *Advanced Healthcare Materials*, 2022, 11 (19), pp.2200195. 10.1002/adhm.202200195 . hal-03808906

HAL Id: hal-03808906

<https://hal.science/hal-03808906>

Submitted on 28 Nov 2022

HAL is a multi-disciplinary open access archive for the deposit and dissemination of scientific research documents, whether they are published or not. The documents may come from teaching and research institutions in France or abroad, or from public or private research centers.

L'archive ouverte pluridisciplinaire **HAL**, est destinée au dépôt et à la diffusion de documents scientifiques de niveau recherche, publiés ou non, émanant des établissements d'enseignement et de recherche français ou étrangers, des laboratoires publics ou privés.



Distributed under a Creative Commons Attribution 4.0 International License

1
2
3
4 **Engineering novel 3D models to recreate high-grade osteosarcoma and its immune and**
5 **extracellular matrix microenvironment**
6

7
8 *Marina Pierrevé¹, Vincent Flacher², Christopher G. Mueller², Romain Vauchelles¹, Eric*
9 *Guerin³, Benoît Lhermitte⁴, Erwan Pencreach³, Andreas Reisch¹, Quentin Muller², Layal*
10 *Doumard², Wacym Boufenghour², Andrey S. Klymchenko¹, Sophie Foppolo¹, Charlotte Nazon⁵,*
11 *Noelle Weingertner⁴, Sophie Martin¹, Claire Briandet⁶, Véronique Laithier⁷, Antonio Di Marco⁸,*
12 *Laurent Bund⁹, Monique Dontenwill¹, Natacha Entz-Werlé^{1,5*}*
13
14
15
16
17

18
19 ¹ *CNRS UMR 7021, Laboratory of Bioimaging and Pathologies, Faculty of Pharmacy, Illkirch,*
20 *France*
21

22 ² *CNRS UPR3572, Laboratory I2CT - Immunology, Immunopathology and Therapeutic Chemistry,*
23 *Strasbourg Drug Discovery and Development Institute (IMS), Institut de Biologie Moléculaire et*
24 *Cellulaire, Strasbourg, France.*
25
26

27 ³ *Department of Cancer Molecular Genetics, Laboratory of Biochemistry and Molecular Biology,*
28 *University Hospital of Strasbourg, France.*
29

30 ⁴ *Pathology department – University Hospital of Strasbourg – France*
31

32 ⁵ *Pediatric Onco-hematology unit – University Hospital of Strasbourg – France*
33

34 ⁶ *Pediatric Onco-hematology unit – Hospital of “Le Bocage”- University Hospital of Dijon –*
35 *France*
36

37 ⁷ *Pediatric Onco-hematology unit – University Hospital of Besançon – France*
38

39 ⁸ *Department of orthopedic surgery and traumatology – University Hospital of Strasbourg –*
40 *France*
41

42 ⁹ *Department of pediatric surgery – University Hospital of Strasbourg – France*
43
44

45
46
47
48 ** Corresponding author*
49

50 *Natacha Entz-Werlé, MD, PhD*
51 *Pediatric Onco-Hematology – University Hospital of Strasbourg*
52 *1 avenue Molière – Strasbourg – 67098 Cédex*
53 *UMR CNRS 7021 – Laboratory of Bioimaging and Pathologies*
54 *74 route du Rhin – 67400 – Illkirch*
55 *Phone: +33 3 88 12 83 96 – Fax: +33 3 88 12 80 92*
56 Natacha.entz-werle@chru-strasbourg.fr
57
58

59 **Keywords:** osteosarcoma, macrophages, hypoxia, 2D culture, spheroid, bone scaffold
60
61
62

Abstract

Osteosarcoma (OS) is the most common primary bone cancer, where overall 5-year surviving rate is below 20% in resistant forms. Accelerating cures for those poor outcome patients remain a challenge. Nevertheless, several studies of agents targeting abnormal cancerous pathways have yielded disappointing results when translated into clinic because of the lack in accurate OS preclinical modeling. So, any effort to design preclinical drug testing might consider all inter-, intra- and extra-tumoral heterogeneities throughout models mimicking extracellular and immune microenvironment. Therefore, we are proposing here the bioengineering of patient-derived models reproducing the OS heterogeneity, the interaction with tumor-associated macrophages (TAMs) and the modulation of oxygen concentrations additionally to recreation of bone scaffold. We, first, developed eight two-dimensional preclinical models mimicking several OS clinical situations and their TAMs in hypoxic conditions and, subsequently, generated the paired three-dimensional (3D) models faithfully preserving histological and biological characteristics. We were in capacity to shape reproducibly M2-like macrophages cultured with all OS patient-derived cell lines in both dimensions. The final 3D models pooling all heterogeneity features are providing accurate proliferation and migration data to understand the mechanisms involved in OS and immune cells/biomatrix interactions and sustained that such engineered 3D preclinical systems will improve personalized medicine.

1. Introduction

Osteosarcoma (OS) is the most common primary bone malignancy that affects adolescents and young adults and is known to be a highly aggressive malignancy.^[1] Commonly, tumors are found near the metaphyseal growth plates of long bones, mostly in the lower limbs.^[2] The OS arises from osteoblastic progenitors unable to proceed to their terminal differentiation, but able to generate new

1
2
3
4 bone tissue and invade the surrounding bone matrix.^[3] Around twenty percent of the patients will
5
6 be diagnosed for visible metastases, whereas more than 80% of them present micro-metastases.^[4]
7
8
9 The current first-line treatment begins with multiagent chemotherapy (ifosfamide, cisplatin,
10
11 doxorubicin, vepeside and/or methotrexate), followed by a surgical resection of the primary tumor
12
13 and an adjuvant chemotherapy adapted to the tumor response to the neoadjuvant therapy.^[5-7] With
14
15 this standard strategy, over the past 30 years, the overall survival of patients with osteosarcoma
16
17 remains stable. All patients with localized primary tumors at diagnosis have a 5-year survival rate
18
19 of more than 60% while patients with a metastatic tumor at diagnosis drop their survival rate to
20
21 20%.^[8] Thus, overall survival must be improved by identifying new therapeutic strategies, which
22
23 notably implies a better understanding of OS chemoresistance. To provide those new insights, it
24
25 is urgently required to develop *in vitro* models integrating the bone specificities and its
26
27 pathophysiological complexity leading to therapeutic resistances. The OS microenvironment is
28
29 surveyed by the immune system through specific macrophages^[9,10] and is characterized by a
30
31 cancerous osteoid matrix,^[11] and an oxygen gradient, ranging from the normal peripheral physioxia
32
33 in bone marrow at 6% of oxygen to a profound hypoxia in the tumor core.^[12,13] The surrounding
34
35 immune microenvironment comprises the tumor-associated macrophages (TAM) and T
36
37 lymphocytes.^[14] Several studies in multiple cancers and in OS have shown that the presence of
38
39 specific TAM is linked with better survival and fewer metastases.^[15] The macrophages present in
40
41 this microenvironment include M1 and/or M2 populations, where M1 are generally defined as pro-
42
43 inflammatory and anti-tumoral macrophages and M2 as anti-inflammatory and pro-tumoral cells.
44
45 However, M2 macrophages appear as the major OS immune cells depending on the tumoral site
46
47 **and seem to be one of the keys in chemoresistance.**^[16-18]
48
49
50
51
52
53
54
55
56
57
58 To mimic these complex features, many laboratories are now focusing on models based on patient-
59
60 derived OS cells.^[19-21] The *in vitro* xenografted animal models are not considering the immune
61
62
63
64
65

1
2
3
4 microenvironment engineering, as fresh OS biopsies and/or OS patient-derived cell lines (PDCL)
5
6 are usually orthotopically or subcutaneously injected in immunodeficient hosts (e.g., nude or NOD
7
8 scid gamma (NSG) mice). Generation of syngenic models in immunocompetent animals could be
9
10 an alternative but are not using human OS cells. Therefore, for now, variations of immune
11
12 microenvironment are not well recreated to study OS origin, progression and response to drugs. To
13
14 mimic osteoid matrix, the use of biomaterials that incorporate physiological components of the
15
16 bone should enable to reproduce its spatial, mechanical, and biological complexity. The
17
18 extracellular matrix (ECM) of bones and cartilages contains mineralized collagen fibers,^[22] as well
19
20 as glycosaminoglycans (GAGs), which are crucial to maintain mechanical properties and cell
21
22 differentiation.^[23,24] Therefore, the combination of collagen with chitosan, a natural polymer with
23
24 a chemical structure similar to GAGs, might recapitulate bone ECM and provide a favorable
25
26 structural support to recreate the physiological mechanical induction and/or the secretion of factors
27
28 for immune and bone cell differentiation, proliferation and migration. Such scaffolds were used by
29
30 the past to mimic the cutaneous matrix in skin models,^[25] but also to take part into new approaches
31
32 developed for osteosarcoma regeneration therapies, as well as inducers of bone differentiation or
33
34 to activate external therapies potentially able to enhance this bone regeneration.^[26-28]

35
36 The aim of our work was to engineer a novel three-dimensional (3D) model considering the bone
37
38 complexity with its ECM, macrophages, hypoxic microenvironment and tumor cells. For this
39
40 purpose and to prepare the validation of this innovative 3D system, we started first to develop
41
42 several PDCLs to take into account inter- and intra-tumoral variations and provide the accurate and
43
44 appropriate clinical situations to study.^[28-30] Next, PDCLs and M2 macrophages were co-cultured
45
46 in hypoxic gradients to create two-dimensional (2D) models and the paired 3D spheroids. The 2D
47
48 step was the prerequisite to validate the characteristics of isolated OS and immune cells and their
49
50
51
52
53
54
55
56
57
58
59
60
61
62
63
64
65

1
2
3
4 co-cultures and be in capacity to maintain those characteristics in 3D systems. To distinguish the
5
6 two cell populations, track cellular movements and assess proliferation we used dye-loaded
7
8 polymer nanoparticles of different colors (NPs),^[31] which can efficiently internalize inside cells by
9
10 endocytosis and provide their long-term labelling.^[32] 3D spheroids were subsequently elaborated
11
12 to construct small tumors where immune and osteosarcoma cells were present and verified the
13
14 maintenance of their characteristics. Finally, we prepared a 3D bone model combining a
15
16 physiologically relevant matrix containing collagen and chitosan and cultured under hypoxia OS
17
18 cells with M2 macrophages. These steps allowed the engineering of more accurate osteosarcoma
19
20 models to use in the future for precision medicine and that were able to pool OS inter-, intra- et
21
22 extra-tumoral heterogeneities.
23
24
25
26
27
28
29
30

31 **2. Results and discussion**

32 33 34 **2.1 2D OS PDCLs and patient-derived subcutaneous xenografts (PDSXs): therapeutic** 35 36 **situations, validation and recreation of high-grade osteosarcoma models.**

37
38 The generation of OS patient-derived models were part of the PEDIAMODECAN (PEDIAtric
39
40 MODEls for CANcer research) program, through which *in vitro* models of several pediatric cancers
41
42 were initiated.^[33] In fact, for bone sarcoma subgroup, twenty OS fresh samples and fifteen Ewing
43
44 sarcomas were collected, dissociated, and passaged in cell culture and/or by subcutaneous
45
46 implantations, as described in Figure 1A. Eight samples were only seeded for *in vitro* culture, 4
47
48 were subcutaneously injected into mice and 8 specimens were concomitantly derived for *in vitro*
49
50 culture and for mouse subcutaneous xenografts. We selected for the 2D and 3D model
51
52 bioengineering those eight specimens where paired OS cell line (OSL) and subcutaneous xenograft
53
54
55
56
57
58
59
60
61
62
63
64
65

1
2
3
4 were initially attempted. Those results are detailed in Figure 1B. The PDCL generation after five
5
6 successive culture passages was successful in 75% (12 out of 16 OS specimens seeded *in vitro*).
7
8 The engraftment efficiency in immunodeficient NSG mice was reaching also 75% (9 out of 12 OS
9
10 subcutaneously engrafted). This patient-derived model efficiency was similar for bone diagnostic
11
12 and lung metastatic OS samples. After initial tumor engraftment, tumors were passaged into NSG
13
14 mice to confirm that the PDSX could be reliably maintained from 5 to 12 passages (average of 7
15
16 passages per PDSX). Subcutaneous tumors reached a size of 1000 mm³ within 4- to 8-months. All
17
18 PDSX tumors were dissected, cryopreserved or processed for histopathology evaluation.
19
20
21
22

23
24 The eight selected OS derivations are listed in Table 1 and presented in Figure 1B, which depicts
25
26 clinical and histological characteristics of the patients, aged from 10 to 18 years old. The clinical
27
28 situations overlapped OS diagnosis, as well as relapsing time. Surgical samples were coming from
29
30 localized (5/8) and metastatic tumors (3/8), which are representing the inter-tumoral heterogeneity
31
32 of OS population. For the subset of the six tumors where PDSXs were successful, dissociated cells
33
34 were adapted for *in vitro* propagation to facilitate the validation of OS characteristics. Those 6
35
36 PDSXs were able to be seeded *in vitro* and further cultured (example of OSL16 in Figure 1C, where
37
38 its paired post-PDSX line is presenting similar microscopic features to the biopsy-derived line).
39
40
41
42 Several passages were confirming the post-PDSX OSL establishment into paired stable cell lines.
43
44
45 So, we were able to generate from those eight OS biopsies 8 stable PDCLs and paired PDSX in 6
46
47 cases (Table 1) and from the 6 subcutaneous xenografts their paired post-PDSX line.
48
49

50
51 Those eight OS PDCLs bear osteoblastic biomarkers shown in Figure 1C for OSL16 with positive
52
53 cytoplasmic immunofluorescent staining of SPARC/osteonectin and osteocalcin. This positivity is
54
55 present in 100% of OS cells. Recently, research results showed that human mesenchymal stromal
56
57 cells (hMSC) are one of the progenitor cells expressing GD2, a neural ganglioside. Such GD2+
58
59 hMSCs during their *in vitro* differentiation interact or become osteoblasts that produce an osteoid
60
61
62
63
64
65

1
2
3
4 matrix. Therefore, we used GD2 immunofluorescent positivity to evaluate and number
5
6 mesenchymal osteoblastic progenitors in our cultures.^[34] GD2 immunolabeling did not stain all OS
7
8 cells but, as shown in Figure 1D on the left images, more than 50% of them have an intense positive
9
10 staining (between 47 to 75% of OS cells in each line).
11
12

13
14 To confirm further the OS characteristics of PDCLs, we used the different lines for *in vivo*
15
16 subcutaneous implantations. As expected, all previous successfully engrafted initial samples had
17
18 paired post-cell line development of subcutaneous tumors in NSG mice. Engraftments of OSL20
19
20 and OSL35 failed in the “standard” direct PDSXs procedure but were successful as post-cell line
21
22 PDSXs. Histopathology of initial and post-cell line PDSXs (Table 1 and Figure 1E) showed typical
23
24 characteristics of pediatric OS, including a high cellularity, varying extent of osteoid matrix (red
25
26 arrows), mitotic activity (black arrows pointing mitotic malignant osteoblasts) and vascularization.
27
28
29 The PDSXs, generated from tumor biopsies or from PDCLs, recapitulated architectural and
30
31 cytologic features seen in the corresponding patient OS from which they were derived.
32
33

34
35 We also performed allelotyping analyses to confirm that PDCLs and PDSXs bear the same DNA
36
37 rearrangements than the paired patient tumor. As described in previous publications from our
38
39 laboratory,^[28,29] several microsatellites located in *TP53* intron 1, close to *p16/INK4a (D9S171)* and
40
41 on chromosome 7 (*D7S2495*, *D7S486* and *D7S1683*) frequently presented an allelic imbalance (AI)
42
43 in the patient tumor comparatively to their normal blood DNA, as seen in Figure 2. 1. As shown in
44
45 Table 1 and Figure 2, all *in vitro* and *in vivo* models matched the AI of the tumors from which they
46
47 were generated. The only differences observed in those DNA analyses are the percentage of OS
48
49 cells presenting this rearrangement in the derived models (Figures 2B and 2C). Indeed, as shown
50
51 for OSL16 and OSL08, the PDCL and/or PDSX had half of their cells bearing the DNA
52
53 rearrangement found in the corresponding patient. This reflects the polyclonality of those models
54
55
56
57
58
59
60
61
62
63
64
65

1
2
3
4 recreating the intra-tumor heterogeneity of pediatric OS. This heterogeneity decreased with the
5 passages (example in OSL18, Figure 2B), suggesting that *in vitro* or *in vivo* expansion of OS cells
6 selected homogeneously mutated tumor cell populations. So, through the monitoring of DNA
7 rearrangements and GD2 staining, we were able to evidence in this osteoblastic population a tumor
8 cell continuum that goes from progenitors to differentiated malignant osteoblasts. Their molecular
9 intra-tumoral heterogeneity was by the past deciphered with CGHarray analyses and recently with
10 RNA sequencing or single cell analyses.^[35] For the microsatellite AI chromosomal location, as
11 expected from previous trials, *TP53* rearrangement and/or its loss of heterozygosity was the more
12 frequent molecular hallmark observed in our PDCL models (6 out of our 8 specific models).^[29,36]
13 When enlarging our OS model population to the 20 attempted derivations, the 15 finalized models
14 (Figure 1B) were presenting this *TP53* abnormality in 80% of cases (12 out of 15).

15
16 In conclusion, we were able to recreate 2D *in vitro* models and PDSXs preserving all osteosarcoma
17 cell features, as well as their intra-tumoral and inter-tumoral heterogeneity. This development was
18 the prerequisite to go further and engineer the hypoxic and immune OS microenvironment in 2D
19 and 3D conditions for those PDCLs. Those models remained rare even a gradually increasing
20 number of recent published researches using PDCLs for drug testing.^[19,37,38]

2.2 2D model engineering and technological developments for the recreation of oxygen and immune osteosarcoma microenvironment.

21
22 The next step to build appropriate 3D system mimicking extra-tumoral heterogeneity was to test
23 the tolerance of hypoxic conditions for OS and macrophagic cells and to be in capacity to co-culture
24 both tumor and immune cells, track them during experiments and evaluate the respective cell-to-
25 cell interactions on proliferation and 3D modelization.

2.2.1 Variable hypoxic conditions of culture and PDCL tolerance

To engineer the hypoxic features of tumor microenvironment and mimic the different tumors areas (e.g., regions well oxygenated close to the vascular space and the hypoxic regions in the tumor core), all eight PDCLs were cultured in parallel at 21%, 5% and 1% O₂. We investigated systematically all cellular changes during approximately 120h using the microscopic acquisitions every 4h by IncuCyte[®] technology and its Zoom Live Cell Analysis system.

As shown for OSL16 in supplemental Figure 1A, the phenotypic aspect of the OS cells and their confluence at the seeding time, or after 48h and 96h were not affected by an intense hypoxia (1% O₂). In addition, we performed proliferation assays using the same IncuCyte[®] system. No significant differences were seen in doubling times when comparing 21% and 1% O₂ for each OS PDCL (Table 1 and examples in supplemental figure 1B). The average doubling time was between 63h and 122h (mean of 85.25h) in normoxia and 59h and 168h in hypoxia (mean of 90.25h). Increased expression of nuclear HIF-1 and of cytoplasmic pS6-RP, reflected activation of the mTor pathway upstream of HIF-1, confirmed the induction of hypoxic signaling in all OS cells under those conditions of oxygen low concentrations (supplemental Figures 1C, right panel), as in tumor samples and in PDSX (supplemental Figures 1C, left panel). Our results are in concordance with recent research publications highlighting the frequent involvement and prognostic impact of hypoxic biomarkers in pediatric osteosarcomas and its correlation with a more aggressive OS cell phenotype.^[13,39,40]

Together, our results demonstrated that all OS PDCLs tolerated well very low oxygen concentrations and were preserving their phenotypic characteristics.

2.2.2 M2 macrophage differentiation in normoxic and hypoxic conditions

1
2
3
4 Macrophages, mainly of M2 phenotype (CD163+/c-MAF+), play a central role in OS response to
5 chemotherapy, as well as in local and metastatic OS progression.^[41-43] In order to clarify and
6 distinguish the roles of M2 macrophages in OS models and disease, we developed a 2D model in
7 both oxygen conditions (21% and 1% O₂) integrating macrophages together with OS PDCLs. To
8 obtain CD163+ macrophages resembling osteoclasts, we differentiated them from circulating
9 monocytes using M-CSF stimulation for 5 days. On images captured by contrast-phase microscope,
10 D5 macrophages acquired a slight but non-significant increase in their diameters and, for a third of
11 them, an elongated global cell shape (supplemental Figures 1D). No difference in adherence was
12 observed during cell passage, nor oxygen modulation. All M2 cells, independently from their
13 morphology, maintained a CD163 and c-MAF staining confirming the stably M2-like phenotype
14 as in previous publications.^[16,17,41,44] The initial generation and isolation of M2 macrophages is a
15 procedure that is quite different from the previous models developed in adult cancer models.^[45-47]

2.2.3 2D co-cultures and cell interactions: viability, hypoxia, nanoparticle (NP) labelling and cancer cell phagocytosis

34
35
36
37
38
39 The next step was to combine those OS and macrophagic cells in a 2D culture system to evaluate
40 their respective viability, hypoxia tolerance and interactions (Figure 3A). In fact, the analysis of
41 cell morphology (Figure 3B, left panel) by contrast-phase microscope did not allow to easily
42 distinguish macrophages from PDCLs, although, upon closer inspection, the former displayed a
43 larger cell diameter and an elongated cell shape and the latter had smaller nucleus. Therefore, we
44 used dye-loaded polymeric NPs of two different colors to label these two cell populations: DiO-
45 loaded NPs labeled the OS PDCL in green, while Cy5 (DiD)-loaded NPs tagged the M2
46 macrophages (D6 of differentiation) in red (Figures 3B), which are standard colors used.^[31,32]

47
48
49
50
51
52
53
54
55
56
57
58
59
60
61
62
63
64
65
66
67
68
69
70
71
72
73
74
75
76
77
78
79
80
81
82
83
84
85
86
87
88
89
90
91
92
93
94
95
96
97
98
99
100
101
102
103
104
105
106
107
108
109
110
111
112
113
114
115
116
117
118
119
120
121
122
123
124
125
126
127
128
129
130
131
132
133
134
135
136
137
138
139
140
141
142
143
144
145
146
147
148
149
150
151
152
153
154
155
156
157
158
159
160
161
162
163
164
165
166
167
168
169
170
171
172
173
174
175
176
177
178
179
180
181
182
183
184
185
186
187
188
189
190
191
192
193
194
195
196
197
198
199
200
201
202
203
204
205
206
207
208
209
210
211
212
213
214
215
216
217
218
219
220
221
222
223
224
225
226
227
228
229
230
231
232
233
234
235
236
237
238
239
240
241
242
243
244
245
246
247
248
249
250
251
252
253
254
255
256
257
258
259
260
261
262
263
264
265
266
267
268
269
270
271
272
273
274
275
276
277
278
279
280
281
282
283
284
285
286
287
288
289
290
291
292
293
294
295
296
297
298
299
300
301
302
303
304
305
306
307
308
309
310
311
312
313
314
315
316
317
318
319
320
321
322
323
324
325
326
327
328
329
330
331
332
333
334
335
336
337
338
339
340
341
342
343
344
345
346
347
348
349
350
351
352
353
354
355
356
357
358
359
360
361
362
363
364
365
366
367
368
369
370
371
372
373
374
375
376
377
378
379
380
381
382
383
384
385
386
387
388
389
390
391
392
393
394
395
396
397
398
399
400
401
402
403
404
405
406
407
408
409
410
411
412
413
414
415
416
417
418
419
420
421
422
423
424
425
426
427
428
429
430
431
432
433
434
435
436
437
438
439
440
441
442
443
444
445
446
447
448
449
450
451
452
453
454
455
456
457
458
459
460
461
462
463
464
465
466
467
468
469
470
471
472
473
474
475
476
477
478
479
480
481
482
483
484
485
486
487
488
489
490
491
492
493
494
495
496
497
498
499
500
501
502
503
504
505
506
507
508
509
510
511
512
513
514
515
516
517
518
519
520
521
522
523
524
525
526
527
528
529
530
531
532
533
534
535
536
537
538
539
540
541
542
543
544
545
546
547
548
549
550
551
552
553
554
555
556
557
558
559
560
561
562
563
564
565
566
567
568
569
570
571
572
573
574
575
576
577
578
579
580
581
582
583
584
585
586
587
588
589
590
591
592
593
594
595
596
597
598
599
600
601
602
603
604
605
606
607
608
609
610
611
612
613
614
615
616
617
618
619
620
621
622
623
624
625
626
627
628
629
630
631
632
633
634
635
636
637
638
639
640
641
642
643
644
645
646
647
648
649
650
651
652
653
654
655
656
657
658
659
660
661
662
663
664
665
666
667
668
669
670
671
672
673
674
675
676
677
678
679
680
681
682
683
684
685
686
687
688
689
690
691
692
693
694
695
696
697
698
699
700
701
702
703
704
705
706
707
708
709
710
711
712
713
714
715
716
717
718
719
720
721
722
723
724
725
726
727
728
729
730
731
732
733
734
735
736
737
738
739
740
741
742
743
744
745
746
747
748
749
750
751
752
753
754
755
756
757
758
759
760
761
762
763
764
765
766
767
768
769
770
771
772
773
774
775
776
777
778
779
780
781
782
783
784
785
786
787
788
789
790
791
792
793
794
795
796
797
798
799
800
801
802
803
804
805
806
807
808
809
810
811
812
813
814
815
816
817
818
819
820
821
822
823
824
825
826
827
828
829
830
831
832
833
834
835
836
837
838
839
840
841
842
843
844
845
846
847
848
849
850
851
852
853
854
855
856
857
858
859
860
861
862
863
864
865
866
867
868
869
870
871
872
873
874
875
876
877
878
879
880
881
882
883
884
885
886
887
888
889
890
891
892
893
894
895
896
897
898
899
900
901
902
903
904
905
906
907
908
909
910
911
912
913
914
915
916
917
918
919
920
921
922
923
924
925
926
927
928
929
930
931
932
933
934
935
936
937
938
939
940
941
942
943
944
945
946
947
948
949
950
951
952
953
954
955
956
957
958
959
960
961
962
963
964
965
966
967
968
969
970
971
972
973
974
975
976
977
978
979
980
981
982
983
984
985
986
987
988
989
990
991
992
993
994
995
996
997
998
999
1000

glycolide) (PLGA) can provide efficient labelling of different cell types through endocytosis without signs of cytotoxicity.^[32] As the color code was preserved inside the cells after several cell divisions, this allowed color barcoding of multiple cell populations and their further long-term tracking.^[30] Here, each cell population was individually labeled with NPs of corresponding color and then these two populations were co-cultured together. Their endocytosis in each cell did not induce any cell mortality and shape modifications (e.g., cell confluence and microscopic follow-up comparing OSLs and M2 macrophages separately and in co-culture with and without labelling as showed in Figure 3B and 3C). Since we did not observe obvious macroscopic differences when different PDCLs were cultured, we choose to focus on OSL16 thereafter. At each step, the IncuCyte® Zoom™ Live Cell Analysis system allowed to monitor cells over time and to demonstrate that the labelled cells could be easily followed and quantified (Figures 3B, top panel). For this purpose, specific IncuCyte® masks were used for image analyses. The NPs remained fluorescent even after 120h of culture for PDCL, which have long doubling-time, to establish clearly their proliferation in the presence of macrophages. The immunofluorescence generated by the NPs in M2 macrophages remained more intense since those cells do not divide (stable number of macrophages on each graph of Figures 3C), limiting the NP dilution over time. Quantification of fluorescent objects confirmed a stable number of M2 macrophages and the concomitant proliferation of OS cells, here exemplified by OSL16 (Figures 3B, right panel). Of note, the co-cultured OS cells proliferated less than in mono-culture (Figures 3C, examples of OSL16, OSL18 and OSL35). This difference may be explained by elimination of OS cells through macrophage phagocytosis, as suggested by the progressive appearance of yellow cells throughout the culture (Figures 3B, bottom row). Indeed, numerous interactions observed between OS cells and macrophages resulted in single yellow cells after few hours. Such events were estimated to concern

1
2
3
4 up to 2.5% cells. Interestingly, this phenomenon was mainly observed in PDCL derived from
5
6 diagnostic tumors. Altogether, fluorescent tracking^[32] afford a close follow-up of both cell
7
8 populations and determine their respective proliferation and interactions. Therefore, it represents a
9
10 valuable tool to monitor co-culture models mimicking the patients' osteosarcoma hypoxic and
11
12 immune microenvironment. For now, only few studies on osteosarcoma were able to approach this
13
14 2D immune modeling and track them easily without any induced-cell mortality.^[48-50] Those 2D
15
16 models can mirror a realistic *in vitro* scenario combining tumor cells and TAMs to be used for the
17
18 study of M2 macrophage depolarization's therapies and/or PDCL drug targeting.^[44]
19
20
21
22
23
24 Nevertheless, these models are lacking the spatial bone environment of the tumor, which governs
25
26 cell-to-cell interactions,^[51] but also the osteoid matrix produced by malignant osteoblast.
27
28
29
30

31 **2.3 3D osteosarcoma models' bioengineering integrating spatial and cell-to-cell interactions** 32 **in a tumoral hypoxic microenvironment** 33

34
35 As stated above, the spatial modelization of cancer models is needed to integrate entirely the extra-
36
37 cellular and cellular microenvironment.^[51,52] For this final purpose, the next step was to introduce
38
39 type I collagen for 3D spatialization of bone scaffold and create spheroids (described in Figure 3A
40
41 and 3D). The final step to develop further the concept of bone matrix was the use of a more complex
42
43 bone-like scaffold adding to collagen chitosan.^[22-25]
44
45
46
47
48

49 *2.3.1 Spheroid or tumoroid modelization in mono- and co-cultures* 50

51 So, we developed a spheroid/tumoroid formation based on OS PDCLs, M2 macrophages and their
52
53 co-cultures within a type I collagen matrix, as described previously.^[22,33] This 3D organization
54
55 allows to shape an oxygen gradient from the periphery to the core of the spheroid, similar to the
56
57 situation within a patient's tumor. We used for this purpose the hanging drop method to be able to
58
59
60
61
62
63
64
65

1
2
3
4 visualize the spheroids and to quantify volume, cell numbers, cellular interactions and the escape
5 and migration into adjacent collagen matrix. The choice of type I collagen, an essential component
6 of the osteoid matrix, was relevant to reflect the biological properties of human bone and
7 understand further the interaction between OS and M2 cells. Mono-cultures and co-cultures were
8 developed into spheric aggregates, as pictured in Figures 3D. M2 macrophage spheroids could be
9 observed after 72h with a large spheroid size ($418.45\mu\text{m} \pm 56.79\mu\text{m}$) (Figures 3D, left panel).
10 They were less compact, more fragile and showed a lower cell density mirroring a loose cell
11 aggregation. In the case of OS cells, we obtained compact and uniformly round spheres after 48h
12 (OSL16, OSL18 and OSL35, Figures 3D, middle panel). No variations between the eight PDCLs
13 could be distinguished microscopically or by sphere size measurement (example of OSL16:
14 $384.97\mu\text{m} \pm 20.87\mu\text{m}$). In the case of spheroids formed from macrophages and PDCL, the
15 morphological aspects of those tumoroids reflected a high density of both cell populations due to
16 strong cell-to-cell interactions, but a smaller global size at 48h of $306.98\mu\text{m} \pm 17.81\mu\text{m}$ (Figures
17 3D, right panel). We expected this multicellular bioengineered tumoroid to be more physiologically
18 relevant, as it reflects the capacity of macrophages and OS cells to invade the bone
19 microenvironment made predominantly of collagen, given the mechanical properties of bone.^[23]
20 Nevertheless, as type I collagen is not the only component of bone matrix, a more complex scaffold
21 was engineered to finalize the 3D system for OS modeling and be able to reproduce both elasticity
22 and toughening of the bone matrix.^[23-25]

2.3.2 Complex bone scaffold engineering provides a 3D microenvironment conducive for immune and osteosarcoma cells interactions and proliferation

We constructed a fully human tissue-engineered bone-mimicking model enabling the investigation of spatial macrophage/osteosarcoma cell interaction (Figure 4A). A rigid scaffold of collagen and

1
2
3
4 chitosan was embedded first with monocytes that were differentiated directly within this matrix,
5
6 using M-CSF as in 2D models or in recent adult models.^[45-47] OS PDCLs were seeded in a second
7
8 step on the opposite side of the matrix. All 3D cultures were done concomitantly in hypoxic and
9
10 normoxic conditions (examples in Figures 4B and 4E). As other natural scaffolds,^[53-55] the
11
12 biocompatibility of our material was maintained for macrophages and all PDCLs. We confirmed
13
14 by confocal microscopy the capacity of isolated OS cells (examples of OSL08, OSL16 and OSL20,
15
16 Figures 4B) to establish and spread throughout the entire thickness of the 3D bone scaffold. We
17
18 analyzed images of immunofluorescent staining revealing cytoplasmic actin (in red) and nuclei (in
19
20 blue, DAPI) of OS cells and macrophages (Figures 4B, 4C and supplementary Videos). The
21
22 scaffold preserved cell morphology depicted in 2D mono- and co-cultures and the ability of
23
24 monocytes to differentiate into CD163+ M2 phenotype (Figures 4D and 4E). We also preserved
25
26 osteoblastic characteristics of all OS PDCLs, as evidenced by SPARC (Figures 4E) and osteonectin
27
28 staining. When focusing on actin filaments fluorescence analysis, we also demonstrated an
29
30 excellent OS cell interaction (Figures 4B) with this bone extra-cellular microenvironment, but also
31
32 an OS cell-macrophage interplay (Figures 4E). Comparatively to single PDCL seeding in the bone
33
34 scaffold, PDCLs plus M2 macrophages appeared with cytoplasmic extensions interconnecting cell-
35
36 to-cell and cell-to-biomaterial. The multicellular scaffolds were embedded in paraffin 3 weeks after
37
38 seeding. Hematoxylin/eosin colorations were examined (Figure 4D, left panel), capturing cell
39
40 proliferation inside the entire matrix and a concomitant migration of immune and cancer cells. To
41
42 validate the presence of M2 macrophages and their cell-to-cell interactions with OS cells, CD163
43
44 immunohistochemical staining was performed on the FFPE multicellular scaffold and
45
46 discriminated CD163+ macrophages from the OS cells (Figures 4D, right panel). Several unstained
47
48 cells (red arrows on Figure 4D) were spread in the scaffold and beside macrophages (black arrows
49
50
51
52
53
54
55
56
57
58
59
60
61
62
63
64
65

1
2
3
4 on Figure 4D) or farther away, recreating cellular and extra-cellular microenvironmental
5
6 components of osteosarcoma more physiologically similar to native tumor tissue and rarely
7
8 reproduced in recent OS models.^[22,23,52]
9

10 11 2.3.3 Estimation of cell-to-cell interaction and OS cell invasion in presence of M2 macrophages

12
13 Both 3D models (e.g., spheroids and bone scaffold systems) were used as tools to evaluate cells'
14
15 interactions in hypoxic and bone microenvironment and to estimate their propensity to invade this
16
17 specific ECM. To capture accurately the cell migration, we focused first on spheroid formation
18
19 where both cell populations were labeled with NPs. We took advantage of this labelling to follow
20
21 and estimate the spheroid size, evolution and how cells may evade the core in profound hypoxia at
22
23 1% O₂. So, we performed the same hanging drop method co-culturing M2 macrophages and OS
24
25 cells (Figure 5A). The drop is coated on collagen I and cell migration was assessed using IncuCyte®
26
27 technology for 96h. By the end of this time period, we observed the decrease of spheroid size and
28
29 a multidirectional spread with a large number of evading cells (Figures 5A and 5B, top panel). The
30
31 reduction of spheroid/tumoroid from H0 to H96 is estimated to 53.88 μm for the condition where
32
33 OSL16 is associated to M2 macrophages. It is concomitant with a progressive decrease of 3D
34
35 spheroid (Figure 5B, 5C and 5D) and an increased number of OS cells migrating at a mean distance
36
37 from the tumoroid of 541.29 μm. The same numbers were calculated for OSL18 plus macrophages
38
39 (supplementary Figure 2) where, globally, the reduction of OSL18 tumoroid is evaluate at 44.51
40
41 μm and is associated to a reduced number of evading cells comparing to the condition without M2-
42
43 like cells. The mean distance reached by OSL18 cells from the tumoroid reached 399.04 μm.
44
45
46
47
48
49
50
51
52

53 Yellow NPs were observed all around the OSL16/M2 tumoroid, suggesting that macrophages
54
55 capture OS cells upon migration. We speculate that the central intense hypoxia could also favor
56
57 cancer cell phagocytosis into the core, but yellow cells can also be interpreted as a central
58
59
60
61
62
63
64
65

1
2
3
4 colocalization of OS cells and M2 macrophages. On Figures 5A, bottom panel, the tumoroid color
5
6 is modified progressively with a predominance of DiO/blue cells at the spheroid periphery.
7

8
9 When comparing to a simpler model using only PDCL-spheroid in hypoxic conditions (Figures 5B
10
11 and 5D, supplementary Figures 2), addition of M2 macrophages seems to influence the size of the
12
13 spheroid recreating the potential impact of immune microenvironment on tumor growth and OS
14
15 cell propension to migrate. A significant difference in spheroid diameters is present at H0 and H96
16
17 between both conditions (e.g., spheroid of OSL16 combined to M2 macrophages and spheroid of
18
19 OSL16 monoculture), with $p=0.005$ and $p=0.01$, respectively. There is also a correlation between
20
21 the presence of M2 macrophages and a higher distance from the spheroid for evading cells (e.g.,
22
23 541.29 μm) comparatively to OSL16 3D monoculture (225.99 μm +/- 144.81 μm). Similar
24
25 differences were evidenced in OSL18 models with smaller numbers of evading cells in presence
26
27 of macrophages, but a more extended migration of those OS cells ($p=0.01$ and $p=0.04$, respectively)
28
29
30

31
32 Altogether, the recreation of such tumoroid represents a physiological system and facilitates
33
34 tracking of proliferation and migration. A complementary estimation into the 3D scaffold of cell
35
36 migration using reconstructing stacks and orthogonal views on ImageJ might confirm as shown in
37
38 Figure 5E both cell movements. In fact, we measured after concomitant CD163 and SPARC
39
40 staining the whole thickness of the scaffold comparatively to the migration thickness of both cell
41
42 populations. This migration thickness was varying depending on the intrinsic OS cell
43
44 characteristics and/or based on the presence of macrophages (from 10.27 to 46.2 μm).
45
46
47
48
49

50
51 Both 3D osteosarcoma models provided complementary and accurate migration data to understand
52
53 the mechanisms involved in OS and immune cells/biomatrix interactions. Such models can
54
55 contribute to overcome the use of simple conventional 2D culture systems and be able to integrate
56
57 all *in vivo* parameters influencing OS cell morphology, proliferation and migration to improve
58
59 personalized medicine.^[54,55] These 3D systems seem to recapitulate bone ECM, as well as hypoxic
60
61
62
63
64
65

1
2
3
4 niche, to be able to deeply analyzed the impact of those microenvironmental features on OS cell
5
6 resistance to past and future therapies.
7
8
9

10 11 **3. Conclusion** 12

13
14 In conclusion, it has been demonstrated that patient-derived 2D models widely adopted for high-
15
16 throughput drug screening, since they are easy to handle, are only recapitulating **intrinsic**
17
18 osteosarcoma cell characteristics. As expected, adding hypoxic features and M2 macrophages, the
19
20 major immune population present in pediatric osteosarcomas, are relevant to mirror
21
22 pathophysiologically cell-to-cell interactions impacting OS cell behavior **and engineer extrinsic**
23
24 **heterogeneity able to modulate response to therapies**. Those results are suggesting that proposing
25
26 such co-cultures is undoubtedly a clear alternative to improve the discovery of effective drugs in
27
28 pediatric osteosarcomas. To go further in developing personalized medicine and bioengineering,
29
30 3D scaffold-based culture models, as well as tumoroid forming cultures, in hypoxia can
31
32 complement and improve our biological studies, as they are covering all osteosarcoma parameters
33
34 leading to therapeutic resistance in patients. **They are integrating the extrinsic mechanical**
35
36 **properties undoubtedly taking part to the initiation and progression of OS.**^[22,23,53] They constitute
37
38 excellent candidates for concomitant identification of novel molecular **pathways and a valuable**
39
40 evaluation of sensitivity to their targeted therapies.
41
42
43
44
45
46
47
48
49

50 **4. Experimental section** 51

52 53 **4.1 Generation of patient-derived cell lines (PDCLs)** 54

55 *4.1.1. PDCL seeding, passages and culture* 56 57 58 59 60 61 62 63 64 65

1
2
3
4 All fresh-collected specimens were obtained after informed consent of parents and patients and
5
6 were anonymized for their analyses. This study was conducted in accordance to the local ethical
7
8 committee approval (declaration number: DC-2017-3090). All patients and their paired-lines and
9
10 xenografts are detailed in Table 1. As depicted in Figure 1, osteosarcoma biopsies are dissected
11
12 and directly shared into pieces for culture seeding and subcutaneous xenografts. The dissected
13
14 sample dedicated to culture is carried out on Hibernate[®] medium (A1247501, Gibco) until the
15
16 following procedure. First, the sample is washed in Dulbecco's Phosphate Buffered Saline (D-PBS,
17
18 Dutscher), cut, resuspended in Hibernate medium and 4mg/mL of type IV collagenase (17104-019,
19
20 Gibco) and dissociated using GentleMACS dissociator (Miltenyi Biotec). The tube containing the
21
22 cells is placed onto a rotator wheel in an incubator at 37°C for 20 minutes. The technique is repeated
23
24 until complete cell isolation and the cell suspensions were then filtered twice, centrifuged for 5 min
25
26 at 1[0 rpm and plated in DMEM/F12 medium (31331-028, Gibco) supplemented with 10%
27
28 decompemented fetal bovine serum (FBS) (Dutscher), 1% MEM non-essential amino acids
29
30 (NEAA) (X0557-100, Dutscher), 1% penicillin-streptomycin (Lonza[™] BioWhittaker[™], Fischer
31
32 Scientific), 1% L-glutamine (L-GLN) (Lonza[™] BioWhittaker[™], Fischer Scientific) and 1%
33
34 amphotericin B (Sigma). The medium is changed in the next day depending on the residual red
35
36 blood cells present in the flask. Finally, when cell confluence reached 90%, a culture passage is
37
38 done after D-PBS wash and adherent cell dissociation with accutase (Sigma) at 37°C. PDCLs were
39
40 then replated in DMEM/F-12 medium (Gibco) supplemented with 10% heat-inactivated FBS
41
42 (Dutscher) and with 1% NEAA (Dutscher). All experiments in PDCLs are performed at less than
43
44 15-line passages.
45
46

47
48 To prepare the 2D and 3D experiments, doubling time calculations were systematically done in an
49
50 incubator (HERAcell VIOS 250i, CO₂ incubator, Thermofischer), where oxygen concentrations
51
52
53
54
55
56
57
58
59
60
61
62
63
64
65

1
2
3
4 were modulated from 1 to 21%. The cell growth was then followed for 7 days using IncuCyte®
5
6 Live Cell technology (Essen BioScience). Pictures were automatically acquired over time and
7
8 quantified with IncuCyte® software. Cell population doubling time was determined using the
9
10 following equation: doubling time (days)= $\ln 2(t-t_0)/\ln(N_t/N_0)$, where t-t₀ is the time of exponential
11
12 growth, N_t and N₀ are cell numbers at time t and t₀, respectively.
13
14

15
16 For all experiments in single culture or in co-culture (see section 4.6), real-time scanned contrast-
17
18 phase images were acquired and analyzed by IncuCyte® ZOOM™ Live Cell Analysis system (Essen
19
20 BioScience).
21
22

23 24 *4.1.2 Patient-derived subcutaneous xenografts (PDSX)*

25
26 Animal experiments were conducted in accordance with French guidelines for animal care, under
27
28 the supervision of authorized investigators, and have been approved by the animal research
29
30 committee (APAFIS #2017021410378167). The NSG (NOD Scid Gamma) mice, 4 to 6 weeks old,
31
32 were purchased from Charles River and maintained under pathogen-free conditions. The fresh
33
34 osteosarcoma samples obtained from biopsies were processed directly after surgery. After
35
36 osteosarcoma tissue wash in DMEM containing antibiotics, they were minced on ice into single-
37
38 cell suspension by gentle pipetting and injected subcutaneously in the right and left flanks of mice.
39
40
41
42
43 Animals were observed every two days for tumor appearance and tumor volume was measured
44
45 with manual caliper. They were systematically sacrificed when flank tumors reached more than
46
47 2000 mm³. The maintenance of subcutaneous xenografts were performed using the same
48
49 procedure, but with the xenografted tumors excised just after animal death. In fact, the fresh
50
51 resected xenografts were dissociated, and passaged into 2–3 recipient mice. Models were
52
53 considered established after successfully engrafting through three passages. A part of those
54
55 subcutaneous xenograft tissues were also used for “secondary” culture seeding, as well as for their
56
57 cryopreservation at -80°C and routine histological analyses.
58
59
60
61
62
63
64
65

1
2
3
4 PDCL cell culture suspensions, as depicted in 4.1 were also injected subcutaneously in mouse
5
6
7 flanks and the same procedure and follow-up were applied to them.
8
9

10 11 **4.2 Histological analyses in paraffin-embedded samples**

12 13 14 *4.2.1 Biopsic and PDSX sample preparations and microscopy*

15
16 For the patient biopsies, the paraffin embedding was performed using the TES99 Madite tissue
17
18 embedding system. The blocks are stored in the Centre de Ressources Biologiques (CRB) of
19
20 University Hospital of Strasbourg. Written informed consent was obtained from patients and/or
21
22 legal guardians for use of tissue for research. This study complies with the Declaration of Helsinki
23
24 and obtained the approval of local ethic committee (RNI 2020 – HUS N°7715). They were cut for
25
26 immunohistochemical analyses with a microtome (Microm HM 355S, Thermo Scientific™). Each
27
28 section was 4- μ m thick and the slides were stored at -20°C. For the PDSX samples, the fresh tumors
29
30 were first included in cassette containing Optimal Cutting Temperature (OCT) mounting media
31
32 (Sakura Tissue-Tek). Their cryosections (7 μ m) were cut using a Leica CM3050S microtome and
33
34 the subsequent SuperFrost®Plus slides were also stored at -20°C until immunohistochemistry.
35
36 Standard hematoxylin and eosin histopathologic preparations of all tissue sections from patient
37
38 tumors and derived PDSXs were reviewed by two board-certified pathologists specialized in
39
40 pediatric cancers.
41
42
43
44
45
46

47 48 *4.2.2 Immunohistochemistry*

49
50 The immunohistochemical staining was performed using an automated tissue staining system
51
52 (BenchMark Ultra Ventana XT, Ventana Medical system) on each tumor and PDSX sections with
53
54 OptiView DAB IHC Detection Kit (detecting mouse IgG, mouse IgM and rabbit primary
55
56 antibodies, Roche Diagnostics). Primary antibodies are anti-CD163 (ab87099 ; 1/200 dilution ;
57
58 Abcam), anti-CD68 (M0814, Clone KP1 ; 1:1000 dilution ; Dako), anti-HIF-1a (ab51608 ; 1:200
59
60
61
62
63
64
65

1
2
3
4 dilution; Abcam) and pS6-RP (4858 ; 1:100 dilution ; Cell Signalling). The staining assessment
5
6 was performed by an expertized pathologist. The scoring system was considering a positive sample
7
8 if staining is detected in more than 5% of cells per core of 1mm.
9

10 11 12 13 14 **4.3 Immunofluorescence (IF) assay on 2D cultures**

15
16 15000 cells per well were seeded onto a 24-well plate containing 12-mm coverslips for 48h or 96h
17
18 at 21% or 1% oxygen. They were fixed in 250 μ L of 4% paraformaldehyde (Electron Microscopy
19
20 Sciences, Thermo Scientific) for 10 minutes at room temperature. After three rinses with 1X D-
21
22 PBS, permeabilization is performed for 2 minutes at room temperature using 250 μ L D-PBS-Triton
23
24 0.1% and with 500 μ L of D-PBS-BSA 3% saturation buffer for 1h. This saturation buffer is D-
25
26 PBS-BSA 3% for all antibodies except for the SPARC antibody, which required HEPES buffer (20
27
28 mM HEPES, 2 mM CaCL₂ and 0.15 M NaCl) for all steps. The primary antibody is then incubated
29
30 overnight at 4°C and the secondary antibody is incubated for 45 min at room temperature. Labeling
31
32 with DAPI (Sc3598) (1:2000) and phalloidin actin (phalloidin-Atto 488 sc3598) (1:2000) is
33
34 performed at the same time during secondary-antibody incubation. The same primary antibodies
35
36 and dilutions, detailed in 4.2.2 section, are used for CD163, CD68, HIF-1 and pS6-RP fluorescent
37
38 staining. Other primary antibodies were anti-GD2 (ab68456; 1:150 dilution; Abcam), anti-SPARC
39
40 (BM2202 ; 1:800 dilution ; Origen), anti-c-MAF (E-7) (sc-518062 ; 1:200 dilution ; Santa Cruz
41
42 Biotechnology) and anti-osteocalcin (23418-1-AP; 1:100 dilution ; Proteintech). The secondary
43
44 antibodies were Alexa Fluor™ 568 goat@rabbit IgG (H&L) (A11011; 1:2000 dilution), Alexa
45
46 Fluor™ 568 goat@mouse IgG (H&L) (A11004; 1:2000 dilution), Alexa Fluor™ 647 goat@rabbit
47
48 IgG (H&L) (A21245; 1:2000 dilution) and Alexa Fluor™ 647 goat@mouse IgG (H&L) (A21236;
49
50 1:2000 dilution) (Thermo Scientific).
51
52
53
54
55
56
57
58
59

60 IF observation was performed using a confocal microscope (LEICA TCS SPE II) with a x63 oil
61
62
63
64
65

1
2
3
4 immersion objective (NA: 1.40 - HCX PL APO CS) or a x20 air objective (NA: 0.7 - HCX PL
5
6 APO CS).
7
8
9

10 11 **4.4 Osteosarcoma cell genomic characterization using allelotyping method** 12

13 DNAs, extracted from patient's blood and tumor, as well as paired PDCL and PDSX specimens,
14 were amplified by PCR using primers from the following microsatellites: *TP53*, *D9S171*, *D7S2495*,
15 *D7S486*, *D7S1683*. The PCR products were analyzed by capillary electrophoresis on ABI
16 PRISM[®] Genetic Analyzer 3100 (Applied Biosystems), as already set up and described in previous
17 work.^[26-28] The genomic data were analyzed with the Genemapper Software (Applied Biosystems)
18 and we focused on allelic imbalance (AI) rearrangements to compare the specimens. A cutoff of
19 20% was used to identify significant AI.
20
21
22
23
24
25
26
27
28
29
30

31 32 33 **4.5 M2 macrophage differentiation** 34

35 Human blood monocytes were isolated at the Laboratory of Immunology, Immunopathology and
36 Therapeutic chemistry (I2CT – CNRS UPR 3572) from human blood. Briefly, peripheral blood
37 mononuclear cells (PBMCs) were enriched by Ficoll density gradient centrifugation from buffy
38 coats obtained from the Etablissement Français du Sang (Strasbourg). Then PBMCs were subjected
39 to Percoll gradient centrifugation, yielding ~70% pure monocytes. Thereafter, monocytes (250000
40 cells/cm²) were seeded in 5mL RPMI medium (R2405, Sigma) supplemented with 10% FBS, 50
41 ng/mL of macrophage colony-stimulating factor (M-CSF) (11343115, ImmunoTools), 1% L-
42 glutamine, 1% amphotericin B and 1% penicillin and streptomycin. 1mL of fresh medium was
43 added every two days. After 5-6 days of differentiation, the resulting macrophages were harvested
44
45
46
47
48
49
50
51
52
53
54
55
56
57
58
59
60
61
62
63
64
65

1
2
3
4 by scraping, then the remaining cells were detached with 1X D-PBS + 2 mM EDTA (Gibco) for
5
6 15-30 min at 37°C. Finally, macrophages were centrifuged for 5 min at 1300 rpm and counted.
7

8
9 A similar process was performed directly into the osteoid scaffolds, described below, where the
10
11 final steps after 5-6 days of differentiation needed another M2 cell validation.
12
13

14 15 16 **4.6 PDCL and macrophage co-cultures and follow-up**

17 18 *4.6.1 2D co-culture*

19
20 As already described above in 4.1.1 and 4.5, patient-derived osteosarcoma cells (PDCs) and
21
22 macrophages were prepared separately for a culture passage. 3000 PDCs and 1500 M2
23
24 macrophages were seeded per well in a 96-well plate with PDCL medium. Cells were followed
25
26 with the IncuCyte® technology in an incubator where the oxygen concentration would vary from 1
27
28 to 21% of oxygen at 37°C.
29
30

31 32 *4.6.2 3D spheroid assay*

33
34 To generate the 3D spheroids, the hanging drop method was employed. 20 µL of 20,000 PDCs
35
36 and/or 10,000 M2 macrophages in corresponding medium were mixed to a 3% methylcellulose
37
38 solution and placed under the lid of the culture plate. Then, lids were inverted and incubated in
39
40 normoxic conditions at 37°C during 48h. Thereafter, the drop is coated on collagen I for the next
41
42 experiments (microscopic aspects and migration assay, see above in 2.3.3 section).
43
44
45

46 47 *4.6.3 Nanoparticles (NPs) for cell identification in 2D cultures and spheroid assays*

48
49 Multicolor labelling of cell populations was achieved with dye-loaded polymeric NPs based on a
50
51 procedure described previously.^[32] Here, poly(lactide-co-glycolide) (PLGA) NPs loaded with salts
52
53 of either DiO or the hydrophobic Cy5 derivative DiD with the bulky hydrophobic counterion F12-
54
55 TPB were used. NPs were prepared through nanoprecipitation of acetonitrile solutions containing
56
57 2 g/L of polymer and 20 mM of dye salt (with respect to the polymer) in 20 mM phosphate buffer
58
59
60
61
62

1
2
3
4 at pH 7.4 yielding a final particle concentration of 0.04 g/L in PLGA. The DiO NPs had a size of
5
6 35 \pm 2 nm (based on dynamic light scattering), an absorbance maximum of 488nm, and a
7
8 maximum emission at 508 nm. Their fluorescence quantum yield (QY) was 14%. The sizes of
9
10 corresponding Cy5 NPs have been determined previously by TEM to be 35 \pm 2 nm (based on
11
12 TEM, error gives width at half maximum). Their absorbance and emission maxima lay at 651 nm
13
14 and 690 nm, respectively, with a QY of 13%. All experiments with NPs were performed in a light-
15
16 sheltered environment. PDCs and macrophages were seeded separately at a cell density of
17
18 approximately 30-50% 24h before addition of NPs. Two washes of the targeted cells were
19
20 performed with opti-MEMTM (11058-021, phenol red and serum free, Gibco) medium.
21
22 Concomitantly, opti-MEMTM medium was removed from the cultured cells and the NPs were
23
24 diluted at 1/10 in the same medium, to yield a final concentration of 0.004 g/L in PLGA. Once NPs
25
26 were diluted, 1 mL of this dilution was added rapidly to the cell wells. DiO NPs were used for
27
28 PDCL fluorescent labelling and Cy5 NPs were used for M2 macrophages. Systematically, a control
29
30 well was filled with opti-MEMTM medium without NPs in each experiment. Next, the NPs and cells
31
32 were incubated at 37°C and 5% CO₂ in light-sheltered conditions. After 3h incubation, the medium
33
34 containing the NPs was removed and two washes were performed with opti-MEMTM. Then, 2mL
35
36 of cell-specific culture medium without phenol red was added. For PDCL, this medium was
37
38 composed of DMEM (1X) (11880-028, Gibco), supplemented with 2.5 mM L-glutamine, 17.5 mM
39
40 D-glucose, 1% NEAA (X0557-100, Dutscher) and 10% FBS. For macrophages, it was comprising
41
42 RPMI (R7509, Sigma) supplemented with 10% FBS, 50 ng/mL M-CSF, 1% L-glutamine, 1%
43
44 penicillin/streptomycin and 1% amphotericin. Cells were incubated overnight at 37°C, 21% O₂,
45
46 5% CO₂. Next day, cells were detached and seeded alone or together in co-culture, either in a 96-
47
48 well glass-bottom plate (P96-1.5H-N, Cellvis) or in spheroid conditions (see 4.6.2). Microscopic
49
50
51
52
53
54
55
56
57
58
59
60
61
62
63
64
65

1
2
3
4 image acquisition was performed using IncuCyte[®] technology and its Zoom Live Cell Analysis
5
6 system, where the red acquisition time is at 400 ms and the green acquisition time is at 800 ms.
7

8 9 *4.6.4 Matrix development and cell seeding*

10
11 The collagen-chitosan scaffolds were produced as previously described.^[25] They were seeded with
12
13 monocytes before M2 differentiation and/or PDCs. For the PDCs, 10⁶ cells are seeded on sterilized
14
15 and rehydrated scaffolds and incubated for 2h at 37°C and 5% CO₂ to allow matrix colonization.
16
17 After this incubation time, 5mL of culture medium is added. In case of single PDCL culture, the
18
19 medium is changed twice a week for 3 weeks. For the monocytes, they are seeded in the matrix
20
21 with macrophage differentiation medium for the next 5-6 days (see 4.5 section).
22
23

24
25 In case of co-culture, the monocytes are seeded, first, as described above. After the 5-6 days of M2
26
27 phenotype differentiation, the medium is removed, and the matrix is gently turned over. The
28
29 PDCLs are, then, seeded and incubated for 2h at 37°C in the center of the dried matrix and the
30
31 PDCL medium is subsequently added as described above for the 3-week incubation at 37°C in
32
33 normoxic or hypoxic conditions.
34
35

36 37 38 *4.6.5 Immunostaining in 3D seeded matrix, image acquisition and 3D confocal reconstruction*

39
40 For immunostaining, as well as for paraffin embedding, the seeded matrix is fixed either after
41
42 macrophage differentiation in case of single culture or after 3 weeks of 3D culture in case of mono-
43
44 or co-cultured PDCLs. The fixation process started with 20 min at room temperature in 4%
45
46 paraformaldehyde, which is followed by three washes with 1X D-PBS. The 3D model is thereafter
47
48 dehydrated in 30% sucrose overnight at 4°C and stored in the same conditions until
49
50 immunofluorescent staining or other procedure.
51
52

53
54 A 0.5 cm wide piece of the seeded matrix is placed in one well of a 96-well plate to be
55
56 permeabilized and saturated for 1h at room temperature in 200μL of 3% D-PBS-BSA. Next, it is
57
58
59
60
61
62

1
2
3
4 incubated overnight at 4°C in 100µL of diluted primary antibody in 3% D-PBS-BSA. This step is
5
6 followed by three washes in 1X D-PBS and secondary antibodies, diluted in saturation buffer as
7
8 described in 4.3, are matched carefully on the matrix for 1h at room temperature in the dark. Finally,
9
10 last washes are performed and the stained matrix is placed in a glue drop (Fluoromount G™,
11
12 Invitrogen) between two coverslips. The image acquisition used a confocal microscope with x20
13
14 lens to make planes on the Z axis (voxel: 0.79µm) and the reconstructed 3D images are based on
15
16 different acquired planes and pooled with the Imaris software.
17
18

21 *4.6.7 Paraffin and OCT embedded 3D matrix*

22
23 The matrix, after removing of its white anchor, can be also embedded in paraffin as depicted in
24
25 4.2.1 section. The inclusion in OCT mounting media is done in object holder, soaked previously in
26
27 liquid nitrogen. In this holder, the 3D matrix is entirely covered by OCT and quickly dipped in
28
29 liquid nitrogen for rapid freezing and placed subsequently in a storage at -80°C. The frozen blocks
30
31 are cut using a cryostat to obtain 10 to 30 µm-thick slides. Hematoxylin eosin and IHC can be
32
33 performed as described in 4.2.2 paragraph.
34
35
36
37
38
39

40 **4.7 Migration assays**

42 *4.7.1 3D spheroid migration assay*

43
44 For this purpose, a coating with 50 µg/mL of bovine type I collagen (5005, Advanced BioMatrix)
45
46 into a 24-well plate is done before spheroid seeding. First, 500 µL of culture medium is added per
47
48 well and then one spheroid is seeded in the center of each well. Migration tests are performed at
49
50 5% CO₂ and 1% or 21% oxygen for 96h. After 96h of migration and adding 500 µL of 1%
51
52 glutaraldehyde, fixation is performed for 30 min at room temperature. Three successive washes are
53
54 thereafter performed with 1X D-PBS and a labelling of cell nucleus with DAPI (1:2000 dilution)
55
56 in 3% BSA D-PBS is done for 45 min at room temperature. Spheroids and the migrating cells are
57
58
59
60
61
62
63
64
65

1
2
3
4 then imaged at 5x (Ph1 Plan-NEOFLUAR 5x/0.15) on an epifluorescence microscope (Axio Zeiss
5
6 NA 0.3 WD 73) equipped with a camera (Camera Moticam Pro 285D 60N-C 2/3' 0.63x 426113).

7
8
9 The number of evading cells, the distance between evading cells and spheroid and the diameter of
10
11 the spheroids were quantified using ImageJ software with a home-made macro called “2D spheres
12
13 dispersion 1.7”.

14 15 16 *4.7.2 Scaffold migration evaluation*

17
18 The thickness of the matrix is measured by multiplying the voxels with the number of slices taken
19
20 by the confocal microscope. Knowing that the average distance between two planes is 0.78 μm .
21
22 This value is verified by performing a 3D reconstruction and an orthogonal view on image J and
23
24 by manually measuring the thickness.
25
26
27
28
29
30

31 **4.8 Statistical analyses**

32
33 GraphPad Prism 6 software was used for comparisons between PDCLs, macrophages and co-
34
35 cultures experiments and non-parametric Kruskal-Wallis test following by Dunn’s multiple
36
37 comparison test were performed. The P-value<0.05 was described as statistically.
38
39
40
41
42

43 **5. Acknowledgements**

44
45 We thank first all children and families affected by osteosarcomas for their contributions to this
46
47 research.
48
49

50 This work was initiated and supported by Satt Conectus program, Fondation de l’Université de
51
52 Strasbourg, “Franck Rayon de Soleil”, “Semeurs d’Etoile”, “Mimi pour la vie” and LifePink
53
54 associations. We are very thankful for their funding and their help for this osteosarcoma study, as
55
56 well as funding from “Jetons contre le Cancer” from Rotary International, Inner Wheel and
57
58 Rotaract associations.
59
60
61
62
63
64
65

1
2
3
4 We also thank Mrs Christelle Lasthaus, Dr Aurélie Nguyen, Mrs Marie Litzler and Mr Aurelien
5
6 Tripp initiating the animal subcutaneous xenografts and bone cell line program into
7
8 PEDIAMODECAN global project. We are also highly thankful to Dr Isabelle Lelong-Rebel for
9
10 cell line development and their improvement.
11
12
13
14
15

16 **6. Conflict of interest**

17
18 A.S.K and A.R. declare that the described nanoparticle-based cell labelling technology is licensed
19
20 by the University of Strasbourg to Lymphobank. The other authors declare no conflict of interest.
21
22
23
24
25

26 **References**

- 27
28 [1] L. Mirabello, R. J. Troisi, S. A. Savage, *Cancer* **2009**, *115*, 1531.
29 [2] G. Ottaviani, N. Jaffe, *Cancer Treat. Res.* **2009**, *152*, 3.
30 [3] J. W. V. de Azevedo, T. A. A. de Medeiros Fernandes, J. V. Fernandes, J. C. V. de
31 Azevedo, D. C. F. Lanza, C. M. Bezerra, V. S. Andrade, J. M. G. de Araújo, J. V.
32 Fernandes, *Oncol Lett* **2020**, *19*, 1099.
33 [4] A. Luetke, P. A. Meyers, I. Lewis, H. Juergens, *Cancer Treat. Rev.* **2014**, *40*, 523.
34 [5] N. Gaspar, B.-V. Occion, H. Pacquement, E. Bompas, C. Bouvier, H. J. Brisse, M.-P.
35 Castex, N. Cheurfa, N. Corradini, J. Delaye, N. Entz-Werlé, J.-C. Gentet, A. Italiano, C.
36 Lervat, P. Marec-Berard, E. Mascard, F. Redini, L. Saumet, C. Schmitt, M.-D. Tabone, C.
37 Verite-Goulard, M.-C. L. Deley, S. Piperno-Neumann, L. Brugieres, *Eur J Cancer* **2018**, *88*,
38 57.
39 [6] P. A. Meyers, C. L. Schwartz, M. Krailo, E. S. Kleinerman, D. Betcher, M. L. Bernstein, E.
40 Conrad, W. Ferguson, M. Gebhardt, A. M. Goorin, M. B. Harris, J. Healey, A. Huvos, M.
41 Link, J. Montebello, H. Nadel, M. Nieder, J. Sato, G. Siegal, M. Weiner, R. Wells, L. Wold,
42 R. Womer, H. Grier, *JCO* **2005**, *23*, 2004.
43 [7] S. Piperno-Neumann, M.-C. Le Deley, F. Rédini, H. Pacquement, P. Marec-Bérard, P. Petit,
44 H. Brisse, C. Lervat, J.-C. Gentet, N. Entz-Werlé, A. Italiano, N. Corradini, E. Bompas, N.
45 Penel, M.-D. Tabone, A. Gomez-Brouchet, J.-M. Guinebretière, E. Mascard, F. Gouin, A.
46 Chevance, N. Bonnet, J.-Y. Blay, L. Brugières, Sarcoma Group of UNICANCER, French
47 Society of Pediatric Oncology (SFCE), French Sarcoma Group (GSF-GETO), *Lancet*
48 *Oncol.* **2016**, *17*, 1070.
49 [8] K. R. Duchman, Y. Gao, B. J. Miller, *Cancer Epidemiol.* **2015**, *39*, 593.
50 [9] W. Hong, H. Yuan, Y. Gu, M. Liu, Y. Ji, Z. Huang, J. Yang, L. Ma, *Cancer Cell Int.* **2020**,
51 *20*, 83.
52 [10] F. C. Kelleher, H. O'Sullivan, *J Adolesc Young Adult Oncol.* **2017**, *6*, 396.
53 [11] F. Bertoni, P. Bacchini, *Eur J Radiol.* **1998**, *27*, S74.
54
55
56
57
58
59
60
61
62
63
64
65

- 1
2
3
4 [12] A. Carreau, B. E. Hafny-Rahbi, A. Matejuk, C. Grillon, C. Kieda, *J Cell Mol Med* **2011**, *15*,
5 1239.
6 [13] Y. Ouyang, H. Li, J. Bu, X. Li, Z. Chen, T. Xiao, *Int J Biol Markers* **2016**, *31*, 229.
7 [14] Y. Inagaki, E. Hookway, K. A. Williams, A. B. Hassan, U. Oppermann, Y. Tanaka, E.
8 Soilleux, N. A. Athanasou, *Clin Sarcoma Res.* **2016**, *6*, 13.
9 [15] C. Dumars, J.-M. Ngyuen, A. Gaultier, R. Lanel, N. Corradini, F. Gouin, D. Heymann, M.-
10 F. Heymann, *Oncotarget* **2016**, *7*, 78343.
11 [16] A. Gomez-Brouchet, C. Illac, J. Gilhodes, C. Bouvier, S. Aubert, J.-M. Guinebretiere, B.
12 Marie, F. Larousserie, N. Entz-Werlé, G. de Pinieux, T. Filleron, V. Minard, V. Minville, E.
13 Mascard, F. Gouin, M. Jimenez, M.-C. Ledele, S. Piperno-Neumann, L. Brugieres, F.
14 Rédini, *Oncoimmunology* **2017**, *6*, e1331193.
15 [17] E. P. Buddingh, M. L. Kuijjer, R. A. J. Duim, H. Bürger, K. Agelopoulos, O. Myklebost, M.
16 Serra, F. Mertens, P. C. W. Hogendoorn, A. C. Lankester, A.-M. Cleton-Jansen, *Clin*
17 *Cancer Res.* **2011**, *17*, 2110.
18 [18] I. Corre, F. Verrecchia, V. Crenn, F. Redini, V. Trichet, *Cells* **2020**, *9*, 976.
19 [19] F. Kito, R. Oyama, M. Sakumoto, M. Takahashi, K. Shiozawa, Z. Qiao, H. Sakamoto, T.
20 Hirose, N. Setsu, A. Yoshida, A. Kawai, T. Kondo, *In Vitro Cell Dev Biol Anim.* **2018**, *54*,
21 528.
22 [20] A. H. P. Loh, E. Stewart, C. L. Bradley, X. Chen, V. Daryani, C. F. Stewart, C. Calabrese,
23 A. Funk, G. Miller, A. Karlstrom, F. Krafcik, D. R. Goshorn, P. Vogel, A. Bahrami, A.
24 Shelat, M. A. Dyer, *Cancer Lett* **2019**, *442*, 262.
25 [21] A. dos Santos Cavalcanti, W. Meohas, G. de O. Ribeiro, A. C. de Sá Lopes, S. Gholamin,
26 M. Razavi, T. Hanae Kasai Brunswick, A. Avan, J. A. Matheus Guimarães, M. E. Leite
27 Duarte, S. A. Kahn, *PLoS One* **2017**, *12*, e0184891.
28 [22] M. Cortini, N. Baldini, S. Avnet, *Frontiers in Physiology* **2019**, *10*, 814.
29 [23] Y. Han, J. Gomez, R. Hua, P. Xiao, W. Gao, J. X. Jiang, X. Wang, *J Mech Behav Biomed*
30 *Mater.* **2021**, *123*, 104766.
31 [24] M. J. Dewey, V. Kollopoulos, M. T. Ngo, B. A. C. Harley, *Materiala (Oxf)* **2021**, *18*,
32 101149.
33 [25] Q. Muller, M.-J. Beaudet, T. De Serres-Bérard, S. Bellenfant, V. Flacher, F. Berthod, *Acta*
34 *Biomaterialia* **2018**, *82*, 93.
35 [26] S. Dong, Y. Chen, L. Yu, K. Lin, X. Wang, *Adv Funct Mater.* **2020**, *30*, 1907071.
36 [27] S. Dong, Y.-N. Zhang, J. Wan, R. Cui, X. Yu, G. Zhao, K. Lin, *J Meter Chem B* **2020**, *8*,
37 368.
38 [28] N. Entz-Werle, T. Lavaux, N. Metzger, C. Stoetzel, C. Lasthaus, P. Marec, C. Kalifa, L.
39 Brugieres, H. Pacquement, C. Schmitt, M.-D. Tabone, J.-C. Gentet, P. Lutz, A. Babin, P.
40 Oudet, M. P. Gaub, F. Perrin-Schmitt, *Neoplasia* **2007**, *9*, 678.
41 [29] N. Entz-Werle, A. Schneider, C. Kalifa, A.-C. Voegeli, M.-D. Tabone, P. Marec-Berard, L.
42 Marcellin, H. Pacquement, P. Terrier, P. Boutard, N. Meyer, M.-P. Gaub, P. Lutz, A. Babin,
43 P. Oudet, *Br J Cancer* **2003**, *88*, 1925.
44 [30] A. Nguyen, C. Lasthaus, E. Guerin, L. Marcellin, E. Pencreach, M.-P. Gaub, D. Guenot, N.
45 Entz-Werle, *Cancers (Basel)* **2013**, *5*, 662.
46 [31] A. Reisch, A.S. Klymchenko, *Small* **2016**, *12*, 1968.
47 [32] B. Andreiuk, A. Reisch, M. Lindecker, G. Follain, N. Peyriéras, J. G. Goetz, A.S.
48 Klymchenko, *Small* **2017**, *13*, 1701582.
49
50
51
52
53
54
55
56
57
58
59
60
61
62
63
64
65

- 1
2
3
4 [33] A.-F. Blandin, A. Durand, M. Litzler, A. Tripp, É. Guérin, E. Ruhland, A. Obrecht, C.
5 Keime, Q. Fuchs, D. Reita, B. Lhermitte, A. Coca, C. Jones, I. L. Rebel, P. Villa, I. J.
6 Namer, M. Dontenwill, D. Guenot, N. Entz-Werle, *Cancers (Basel)* **2019**, *11*, E1875.
7
8 [34] C. Martinez, T. J. Hofmann, R. Marino, M. Dominici, E. M. Horwitz, *Blood* **2007**, *109*,
9 4245.
10 [35] Y. Zhou, D. Yang, Q. Yang, X. Lv, W. Huang, Z. Zhou, Y. Wang, Z. Zhang, T. Yuan, X.
11 Ding, L. Tang, J. Zhang, J. Yin, Y. Huang, W. Yu, Y. Wang, C. Zhou, Y. Su, A. He, Y.
12 Sun, Z. Shen, B. Qian, W. Meng, J. Fei, Y. Yao, X. Pan, P. Chen, H. Hu, *Nat Commun*
13 **2020**, *11*, 6322.
14
15 [36] J. L. Rokita, K. S. Rathi, M. F. Cardenas, K. A. Upton, J. Jayaseelan, K. L. Cross, J. Pfeil,
16 L. E. Egolf, G. P. Way, A. Farrel, N. M. Kendsersky, K. Patel, K. S. Gaonkar, A. Modi, E.
17 R. Berko, G. Lopez, Z. Vaksman, C. Mayoh, J. Nance, K. McCoy, M. Haber, K. Evans, H.
18 McCalmont, K. Bendak, J. W. Böhm, G. M. Marshall, V. Tyrrell, K. Kalletla, F. K. Braun,
19 L. Qi, Y. Du, H. Zhang, H. B. Lindsay, S. Zhao, J. Shu, P. Baxter, C. Morton, D.
20 Kurmashev, S. Zheng, Y. Chen, J. Bowen, A. C. Bryan, K. M. Leraas, S. E. Coppens, H.
21 Doddapaneni, Z. Momin, W. Zhang, G. I. Sacks, L. S. Hart, K. Krytska, Y. P. Mosse, G. J.
22 Gatto, Y. Sanchez, C. S. Greene, S. J. Diskin, O. M. Vaske, D. Haussler, J. M. Gastier-
23 Foster, E. A. Kolb, R. Gorlick, X.-N. Li, C. P. Reynolds, R. T. Kurmasheva, P. J. Houghton,
24 M. A. Smith, R. B. Lock, P. Raman, D. A. Wheeler, J. M. Maris, *Cell Rep.* **2019**, *29*, 1675.
25
26 [37] C. Zucchini, M. C. Manara, C. Cristalli, M. Carrabotta, S. Greco, R. S. Pinca, C. Ferrari, L.
27 Landuzzi, M. Pasello, P.-L. Lollini, M. Gambarotti, D. M. Donati, K. Scotlandi, *J Exp Clin*
28 *Cancer Res.* **2019**, *38*, 503.
29
30 [38] T. Higuchi, J. Yamamoto, N. Sugisawa, Y. Tashiro, H. Nishino, N. Yamamoto, K. Hayashi,
31 H. Kimura, S. Miwa, K. Igarashi, M. Bouvet, S. R. Singh, H. Tsuchiya, R. M. Hoffman,
32 *Cancer Genomics Proteomics.* **2020**, *17*, 35.
33
34 [39] F. Jiang, X.-L. Miao, X.-T. Zhang, F. Yan, Y. Mao, C.-Y. Wu, G.-P. Zhou, *J Immunol Res.*
35 **2021**, *2021*, 5523832.
36
37 [40] J. Adamski, A. Price, C. Dive, G. Makin, *PLoS One* **2013**, *8*, e65304.
38
39 [41] A. Gomez-Brouchet, J. Gilhodes, N. van Acker, R. Brion, C. Bouvier, P. Assemat, N.
40 Gaspar, S. Aubert, J.-M. Guinebretiere, B. Marie, F. Larousserie, N. Entz-Werlé, G. de
41 Pinieux, E. Mascard, F. Guoin, P. Brousset, M.-D. Tabone, M. Jimenez, M.-C. L. Deley, J.-
42 Y. Blay, L. Brugieres, S. Piperno-Neumann, F. Rédini, *Cancers* **2021**, *13*, 13030423.
43
44 [42] T. Ohba, H. A. Cole, J. M. M. Cates, D. A. Slosky, H. Haro, T. Ando, H. S. Schwartz, J. G.
45 Schoenecker, *J Bone Miner Res.* **2014**, *29*, 1431.
46
47 [43] A. Labrinidis, S. Hay, V. Liapis, D. M. Findlay, A. Evdokiou, *Int J Cancer* **2010**, *127*, 345.
48
49 [44] M. Sylvestre, C.A. Crane, S.H. Pun, *Adv. Mater.* **2019**, *32*, e1902007.
50
51 [45] K. M. Tevis, R. J. Cecchi, Y. L. Colson, M. W. Grinstaff, *Acta Biomater.* **2017**, *12*,
52 e0182039.
53
54 [46] J. Kuen, D. Darowski, T. Kluge, M. Majety. *PLoS One* **2017**, *12*, e0182039.
55
56 [47] S. P. Rebetlo, C. Pinto, T. R. Martins, N. Harrer, M. F. Estrada, P. Lova-Alvarez, J.
57 Cabecadas, P. M. Alves, E. J. Gualda, W. Sommergruber, C. Brito, *Methods Mol Biol.* **2019**,
58 *1882*, 73.
59
60 [48] F. Mahyudin, H. Yazid, M. Edward, M. H. Basuki, Y. A. Bari, F. A. Rantam, *J Adv Pharm*
61 *Technol Res.* **2020**, *11*, 213.
62
63 [49] C. Maloney, M. P. Kallis, M. Edelman, C. Tzanavaris, M. Lesser, S. Z. Soffer, M. Symons,
64 B. M. Steinberg, *Mol Cancer Ther.* **2020**, *19*, 1340.
65

- 1
2
3
4 [50] A. L. Gamblin, A. Renaud, C. Charrier, P. Hulin, G. Louarn, D. Heymann, V. Trichet, P.
5 Layrolle, *Acta Biomater.* **2014**, *10*, 5139.
6 [51] P.S. Takhuri, C. Liu, G.D. Luker, H. Tavana. *Adv Healthc Mater.* **2018**, *7*, e1700980.
7 [52] J. Munoz-Garcia, C. Jubelin, A. Loussouarn, M. Goumard, L. Griscom, A. Renodon-
8 Cornière, M.-F. Heymann, D. Heymann, *J Bone Oncol.* **2021**, *30*, 100379.
9 [53] A. Villasante, A. Marturano-Kruik, S. T. Robinson, Z. Liu, X. E. Guo, G. Vunjak-
10 Novakovic, *Tissue Eng Part C Methods* **2017**, *23*, 98.
11 [54] G. Bassi, S. Panseri, S. M. Dozio, M. Sandri, E. Campodoni, M. Dapporto, S. Sprio, A.
12 Tampieri, M. Montesi, *Sci Rep.* **2020**, *10*, 22294.
13 [55] A. Bozorgi, L. Sabouri, *Cancer Treat Res Commun.* **2021**, *27*, 100324.
14
15
16
17
18
19

20 **Legends:**

21
22 **Table 1:** Summary of clinical data, microscopic aspects, histopathology, molecular and cellular
23 characteristics in the 8 patient tumors and their paired PDCL (patient-derived cell line) and PDSX
24 (patient-derived subcutaneous xenograft).
25
26
27
28
29
30
31

32 **Figure 1: Osteosarcoma patient-derived cell lines (PDCLs) and patient-derived subcutaneous**
33 **xenografts (PDSX) preserved the histological and biological characteristics of this pediatric**
34 **malignant bone cancer. (A) Schematic presentation summarizing the seeding and culture of**
35 **PDCLs and PDSX generation.** After biopsy, the tumor is either directly xenografted
36 subcutaneously in mice or derived in cell lines. **(B) Results obtained in the 20 OS samples where**
37 **the OS cells of the biopsic specimens were seeded and/or subcutaneously xenografted. Finally, 12**
38 **PDCLs and 9 PDSXs were stably generated. (C) Microscopic views of OSL (OSteosarcoma**
39 **Line) 16 (e.g., from right to left side, a focus with a magnification 100x, OSL16 line derived**
40 **directly from the biopsic sample and from PDSX sample with a magnification 20x). (D) Positive**
41 **immunodetection of osteoblastic biomarkers in green (e.g., from right to left side: SPARC,**
42 **osteocalcin and GD2) with confocal microscope (Scalebar=50µm) in an example of OSL16 line.**
43 **A larger view of GD2 immunofluorescent cells is showed at the left end (Scalebar=30µm). Cell**
44
45
46
47
48
49
50
51
52
53
54
55
56
57
58
59
60
61
62
63
64
65

1
2
3
4 nuclei (in blue) and actin (in red) were stained using DAPI and phalloïdin, respectively. (E)
5
6 **Hematoxylin/eosin coloration of diagnostic patient tumors, PDSXs and post-PDCL**
7 **xenografts** for OSL05 and OSL16 lines (Scalebar=50µm). Patient-derived tumor models are
8
9 characterized by a high cellularity, mitotic malignant osteoblasts (black arrows) associated with an
10
11 osteoid matrix (red arrows).
12
13
14
15
16
17
18

19 **Figure 2: Molecular assessment comparing normal blood DNA and the paired diagnostic**
20 **tumor, cell line (OSL) and patient-derived subcutaneous xenograft (PDSX). (A) Example of**
21 **allele 1 and 2 presence in OSL05 patient sample and the paired models. (B) Diagrams**
22 **depicting the DNA levels of several alleles (in percent) in patient's blood (in blue color, as**
23 **expected 100% of both alleles), in tumors (in red color, complete loss of heterozygosity), in PDCLs**
24 **(in green color, variability depending on line and its heterogeneity) and PDSX DNA (in purple**
25 **color, variability depending on PDSX tumor heterogeneity). From the top to the bottom of the**
26 **figure, the molecular results of OSL04, OSL05, OSL08, OSL15, OSL16 and OS118 derivations are**
27 **presented and expressed in percent. (C) Table summarizing the results in each biopsy and its**
28 **paired PDCL and PDSX for each microsatellite.**
29
30
31
32
33
34
35
36
37
38
39
40
41
42
43
44
45

46 **Figure 3: 2D and 3D osteosarcoma models recreating intra-tumoral M2 macrophage and**
47 **hypoxic microenvironment. (A) Schematic representation of osteosarcoma-PDCL and M2**
48 **macrophage co-cultures in 2D and 3D conditions. (B) Contrast-phase view and fluorescent**
49 **follow up of macrophage/PDCL interactions** showing images of adherent OSL16 cells and
50
51 macrophages labelled with fluorescent nanoparticles. Macrophages are dyed in red color and
52
53 osteosarcoma cells in green (first row). The picture at the end of second row is showing DiO (blue
54
55 color) and Cy5 (yellow color) IncuCyte® masks used to differentiate osteosarcoma patient-derived
56
57
58
59
60
61
62
63
64
65

1
2
3
4 cells and M2 macrophages, respectively, in the 2D culture. The images of last row are focusing on
5
6 yellow dots' generation, which are representing M2 macrophages after their phagocytosis of
7
8 osteosarcoma cells. In the central and right pictures, time-lapse visualization of this phagocytic
9
10 mechanism with first M2 macrophage and OSL16 interaction and, 5 hours later, a complete
11
12 phagocytosis of the tumor cell. **(C) Graphs representing PDCL in mono- and co-culture and**
13
14 **M2-like cells** to illustrate the stable numbers of M2 macrophages (in red) and the decrease numbers
15
16 of OSL16, OSL18 and OSL35 cells (in green) per well over time. On the 3 graphs, the comparison
17
18 with mono-culture of OSL lines is confirming the progressive phagocytosis of OS cells in presence
19
20 of M2 macrophages, which is reproducing minimally the immune macrophagic cytotoxicity. **(D)**
21
22 **Microscopic views of spheroids/tumoroids** generated from M2 macrophages (left panel) at 3
23
24 days, from PDCLs (examples of **OSL16, OSL18 and OSL35** in the middle) and from
25
26 macrophage/PDCL co-culture recreating small tumors at 48h (**right panel**).

27
28
29
30
31
32
33
34
35
36 **Figure 4: Bioengineering of extracellular microenvironment (bone scaffold and hypoxia)**
37
38 **associating immune and osteosarcoma cells.** (A) Schematic representation showing the 5-step
39
40 procedure to generate the 3D co-culture model into the bone scaffold. **(B) Immunodetection of**
41
42 **OSL08, OSL16 and OSL20 cells seeded in the 3D bone scaffold** focusing on cytoplasmic actin
43
44 staining in red inside the entire bone scaffold (**nuclei are in blue**). **Representations of experiments**
45
46 **in normoxic and hypoxic conditions.** **(C) Confocal images of M2 macrophage differentiation**
47
48 **and culture in the 3D matrix.** Immunofluorescence is detecting the M2 phenotype biomarker
49
50 CD163 (in cyan color). The cell nuclei are in blue and cytoplasmic actin is stained in green. **(D)**
51
52 **Hematoxylin/eosin staining on a cross section of the 3D scaffold seeded with M2 macrophages**
53
54 **and osteosarcoma cells** on the left side and the immunohistochemical CD163 staining
55
56 differentiating macrophages (black arrows) from osteosarcoma cells (red arrows) on the right side
57
58
59
60
61
62
63
64
65

1
2
3
4 (magnification 40x). **(E) Concomitant immunodetection of M2 macrophage (CD163**
5 **biomarker in red color) and osteosarcoma cells (OSL16 and OSL18) (SPARC biomarker in**
6 **red color) during their co-culture in the scaffold.**
7
8
9

10
11
12
13 **Figure 5: Migration assessment in 3D spheroid models and bone scaffold co-culturing M2**
14 **macrophages and osteosarcoma cells. (A) In the first row, phase-contrast pictures of spheroids**
15 **combining OSL16 cells and M2 macrophages at H0 and H96. In second row, using IncuCyte®**
16 **technology, generation of images showing the progressive migration of PDCLs (labeled with green**
17 **particles) from the spheroid, where M2 macrophages (labeled with red particles) are tightly**
18 **interconnected with osteosarcoma cells in the core of the tumoroid. The last row is representing in**
19 **blue and yellow the IncuCyte® mask measuring cell confluence of PDCLs and macrophages,**
20 **respectively. (Scalebars=600µm). (B) Precise measures of evading/migrating M2 and PDCL**
21 **cells using confocal images of the spheroid at H96 with a DAPI labeling comparing OSL16**
22 **spheroid to M2/OSL16 spheroid. The size of spheroids is decreasing over time with the spread**
23 **of osteosarcoma cells and the OS cell phagocytosis. (C) Bar graph representation underlining**
24 **the significant differences between spheroids containing M2 macrophages plus OSL16 and**
25 **spheroids with mono-cultured OSL16 (*p=0.005, **p=0.01) M2 macrophages are stable,**
26 **whereas OSL16 cells are progressively decreasing as depicted in 2D culture. (D) Table**
27 **summarizing the numbers of evading cells, spheroid diameters and distance mean between**
28 **the periphery of the spheroid and the evading cells. (E) Reconstructed confocal images of the**
29 **bone scaffold thickness looking to the macrophage (in red color) and the osteosarcoma cell**
30 **(in green color) migration into the bone scaffold. The total thickness of the infiltrated scaffold**
31 **is at 26.36µm (10.27µm to 46.2µm).**
32
33
34
35
36
37
38
39
40
41
42
43
44
45
46
47
48
49
50
51
52
53
54
55
56
57
58
59
60
61
62
63
64
65

1
2
3
4 **Supplemental Figure 1: Extracellular and immune microenvironment engineering in 2D**
5 **cultures of osteosarcoma PDCLs. (A) Microscopic views of OSL16 line at 0, 48 and 96 hours**
6 **exposed to normoxic (21% oxygen) and hypoxic (1% oxygen) conditions (Scalebars=300µm).**
7
8
9
10
11 (B) Graphical representations of normalized cell confluence of OSL16, OSL18 and OSL35 in both
12 oxygen concentrations showing no significant proliferative rate differences. (C) **Hypoxic**
13 **biomarker induction.** HIF-1 and pS6 immunohistochemical expressions in biopsic and PDSX
14 samples of OSL16 (20x) and their immunodetection by confocal microscopy in the example of
15 OSL16 cells cultured in hypoxia. HIF-1 and pS6 are stained in green, nuclei in blue and actin in
16 red (Scalebars=50µm). (D) **Macrophage differentiation into M2 phenotype.** Here, all images are
17 captured in hypoxic conditions. On the left side, contrast-phase images of macrophages at day 0
18 (D0) and day 5 (D5) of their M2 differentiation (Scalebars=100µm). On the right side, images
19 (magnification 63x) of M2 polarity macrophages expressing at the cell membrane CD163 (in cyan)
20 and c-MAF (in orange) markers. The cell nuclei are in blue. (Scalebar=50µm).

21
22
23
24
25
26
27
28
29
30
31
32
33
34
35
36
37
38 **Supplemental Figure 2: Complementary data on migration assays in OSL18 line pooling in**
39 **(A) measures of evading/migrating PDCL cells using confocal images of the spheroid at H96**
40 **with a DAPI labeling comparing OSL18 spheroid to M2/OSL18 tumoroid. (B) Table**
41 **summarizing measures of evading cells, spheroid diameters and distance mean between the**
42 **periphery of the spheroid and the evading cells.**

43
44
45
46
47
48
49
50
51
52
53 **Supplemental Videos obtained after reconstruction of the 3D-based scaffold culture's stacks**
54 **with Imaris software.** Immunofluorescent staining is as follows: nuclei are in blue (DAPI),
55 SPARC and actin localized in osteosarcoma cells are in green and CD163+ macrophages are
56 labeled in red. One example of OS116 plus macrophages and another with OSL20 culture.

1
2
3
4
5
6
7
8
9
10
11
12
13
14
15
16
17
18
19
20
21
22
23
24
25
26
27
28
29
30
31
32
33
34
35
36
37
38
39
40
41
42
43
44
45
46
47
48
49
50
51
52
53
54
55
56
57
58
59
60
61
62
63
64
65

20
21
22
23
24
25
26
27
28
29
30
31
32
33
34
35
36
37
38
39
40
41
42
43
44
45
46
47
48
49
50
51
52
53
54
55
56
57
58
59
60
61
62
63
64
65

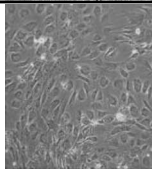
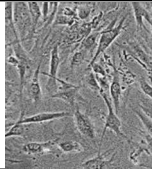
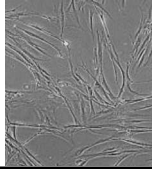
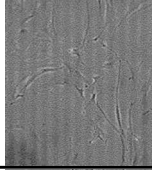
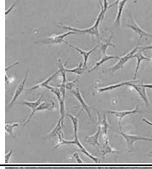
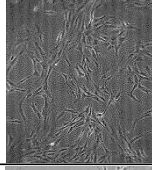
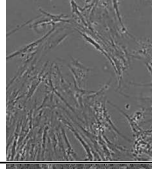
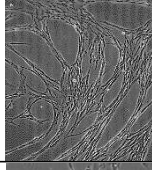
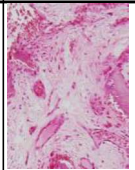
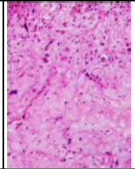
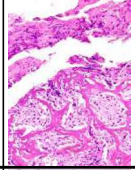
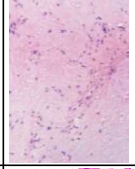
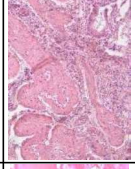
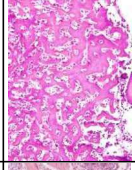
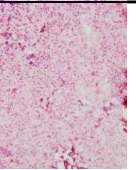
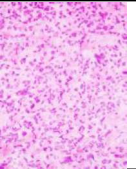
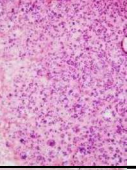
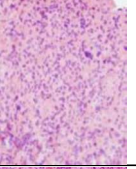
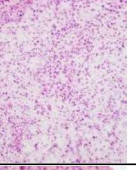
cell lines	OSL04	OSL05	OSL08	OSL15	OSL16	OSL18	OSL20	OSL35
time and location of model generation	diagnostic tibia	pulmonary relapse	pulmonary relapse	diagnostic femur	diagnostic tibia	diagnostic femur	diagnostic femur	pulmonary relapse
patient/tumor characteristics	15 Y GR localized alive	14 Y PR metastatic deceased	17 Y GR localized deceased	10 Y GR metastatic alive	14 Y GR localized alive	15 Y PR localized alive	16 Y PR metastatic deceased	18 Y GR localized alive
cell microscopic aspect								
bone diagnostic biopsy								
paired PDSX								
molecular follow-up	AI TP53+ AI D7S2495+	AI TP53+	AI TP53+ AI D7S486+	AI D7S2495+	AI D9S171+	AI TP53+	AI TP53+	AI TP53+
doubling time (hour)	71h 68h	106h 111h	63h 68h	69h 59h	69h 71h	102h 98h	122h 168h	80h 79h
		21% O ₂						
		1% O ₂						

Table 1: Summary of clinical data, microscopic aspects, histopathology, molecular and cellular characteristics in the 8 patient tumors and their paired PDCCL (patient-derived cell line) and PDSX (patient-derived subcutaneous xenograft).

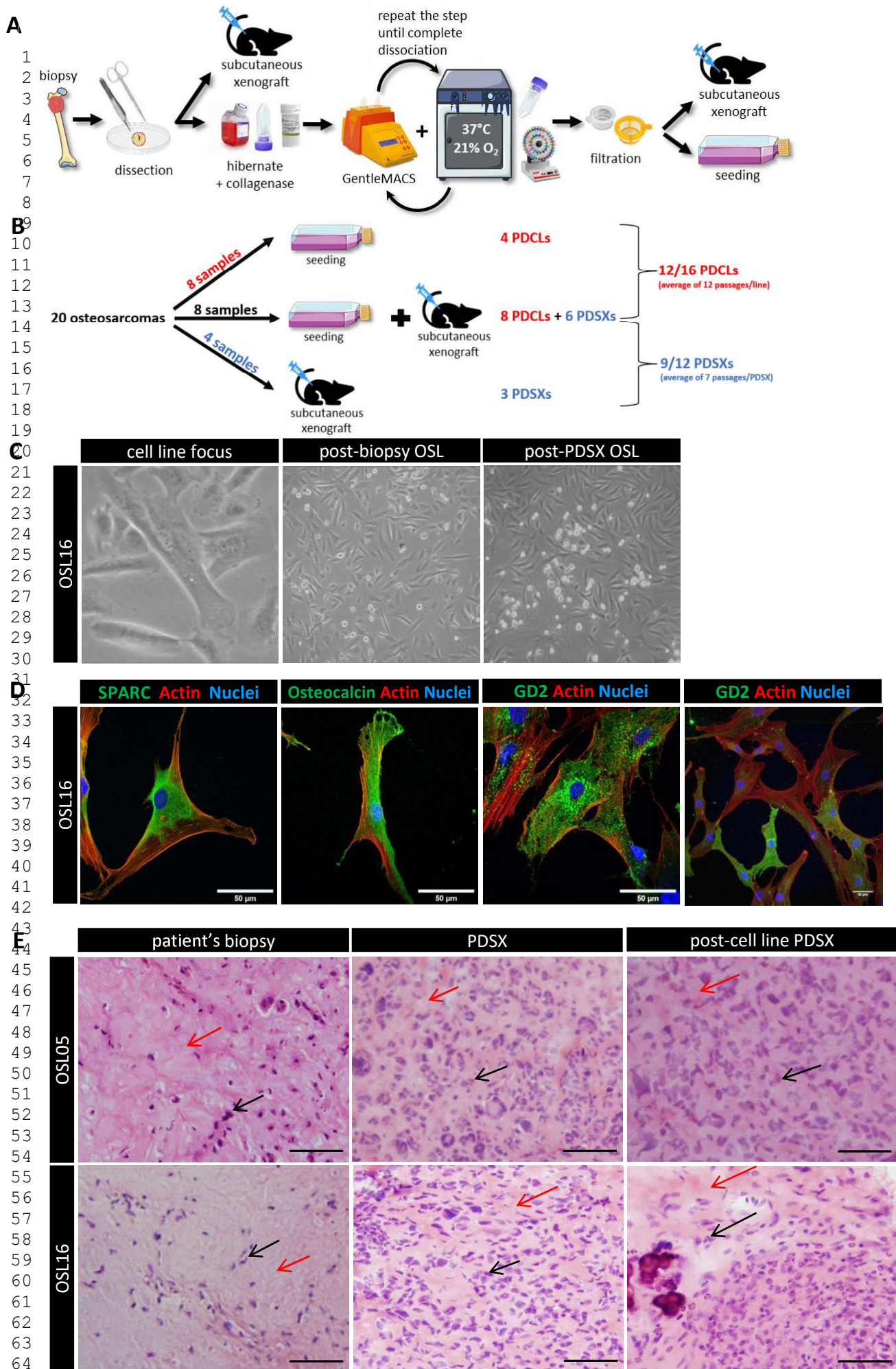
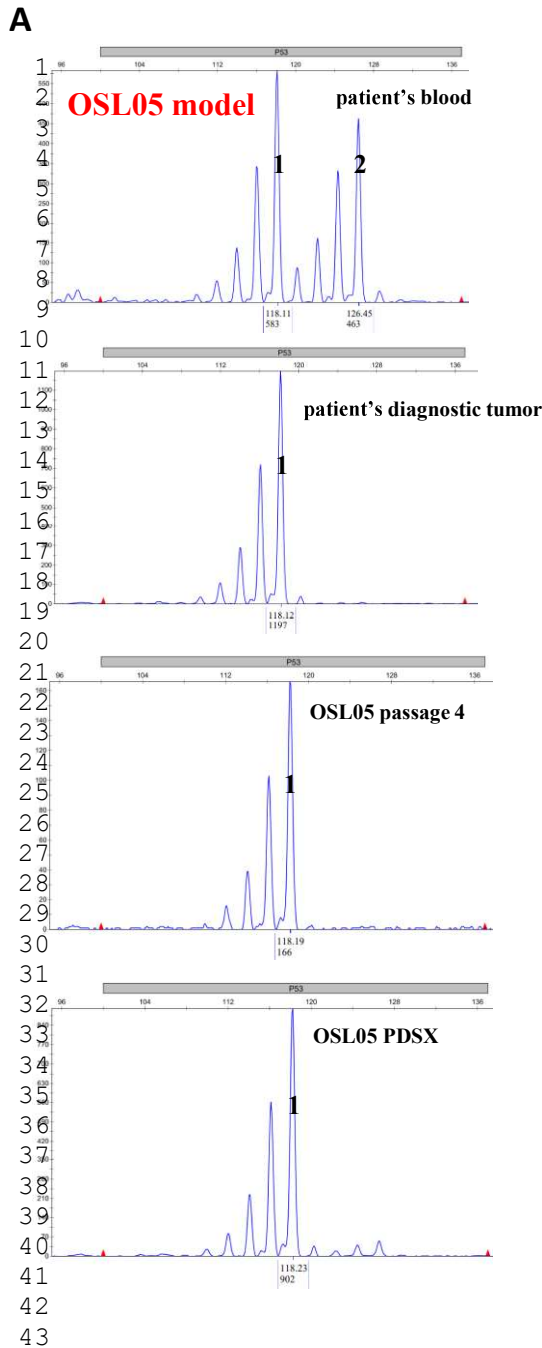


Figure 1 : Osteosarcoma patient-derived cell lines (PDCLs) and patient-derived subcutaneous xenografts (PDSX) preserved the **microscopic** and histological characteristics of this pediatric malignant bone cancer.



C

	tumor sample	PDCL	PSDX
45	OSL04		
46	TP53	0%	2%
47	D7S2495	5%	8%
48	OSL05		
49	TP53	0%	2%
49	OSL08		
50	TP53	2%	12%
51	D7S486	5%	15%
52	OSL15		
53	D7S2495	5%	24%
54	OSL16		
54	D9S171	2%	38%
55	OSL18		
56	TP53	7%	11%
57	OSL20		
58	TP53	8%	NA
59	OSL35		
60	TP53	4%	NA

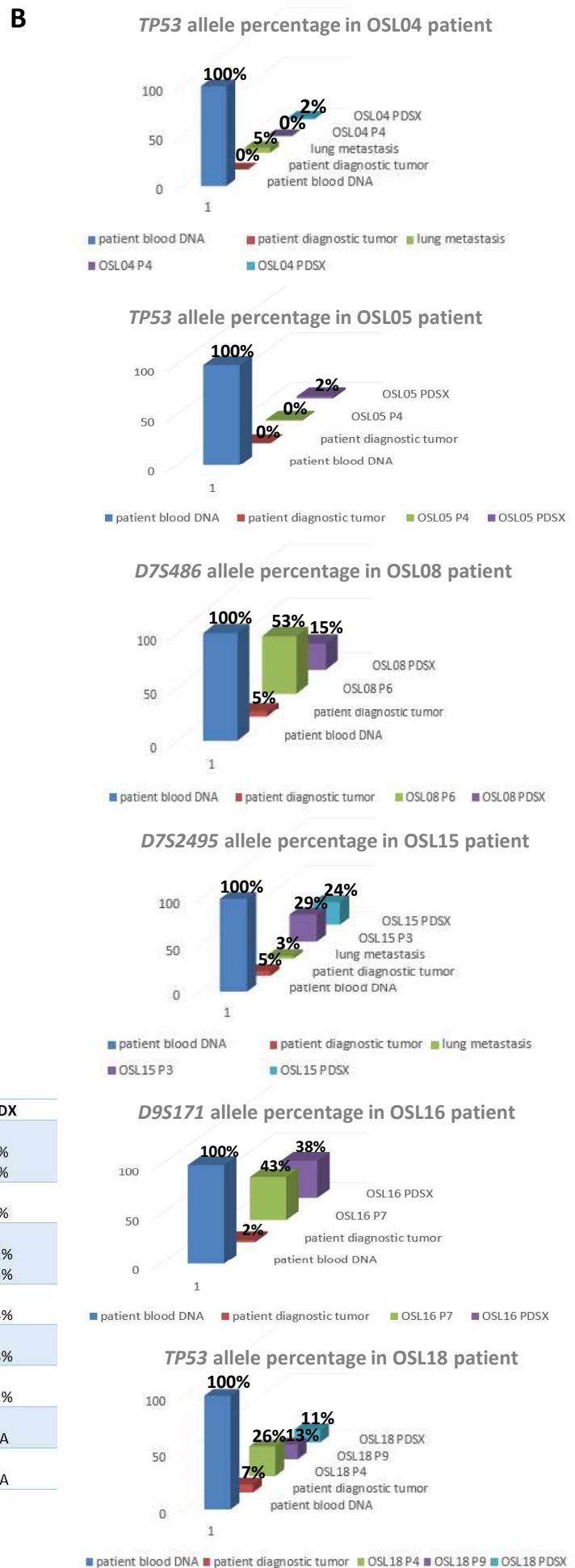
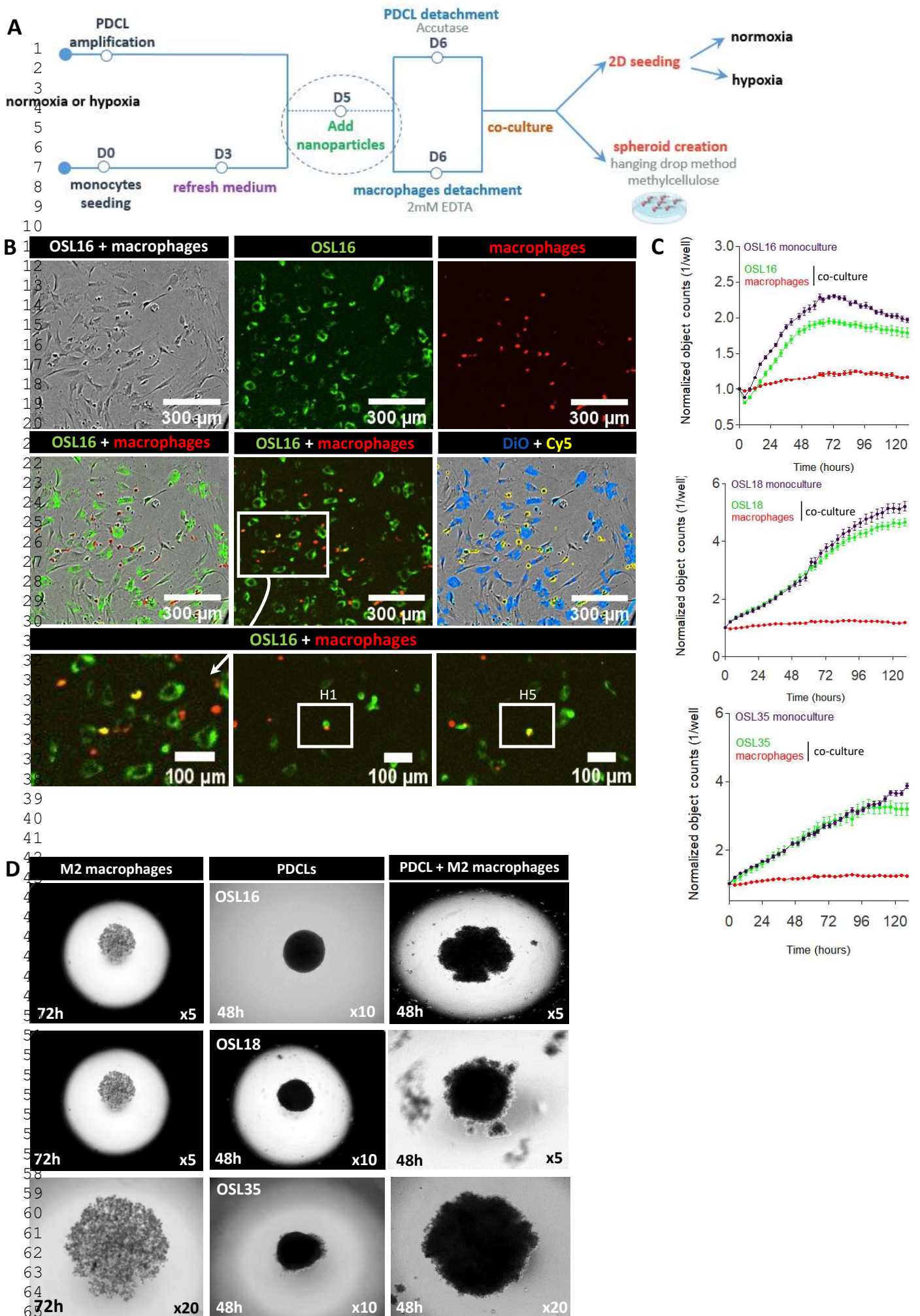


Figure 2: Molecular assessment comparing normal blood DNA and the paired diagnostic tumor, cell line (OSL) and patient-derived subcutaneous xenograft (PDSX).



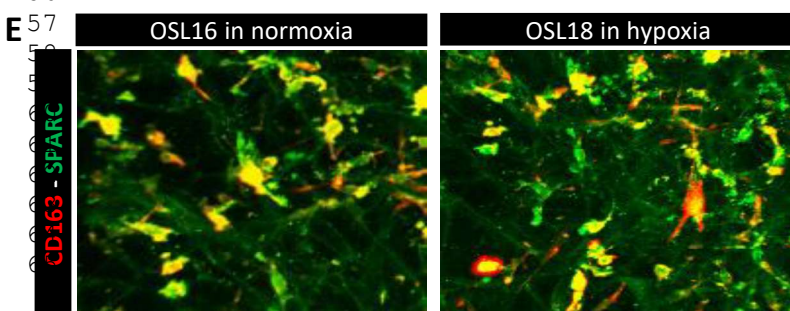
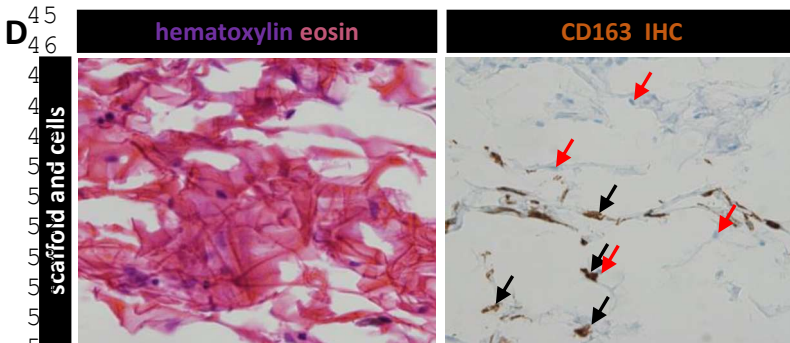
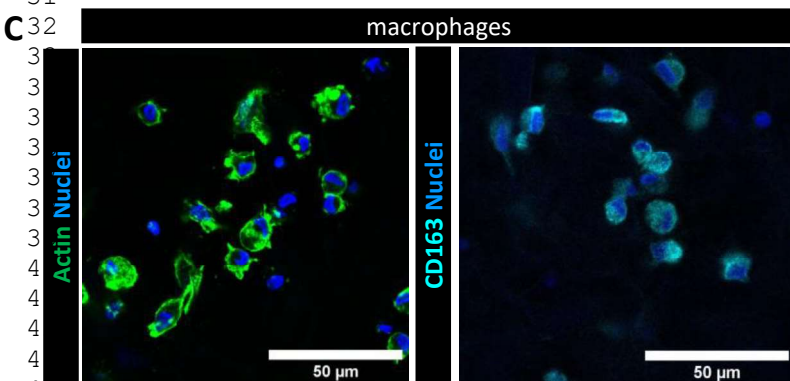
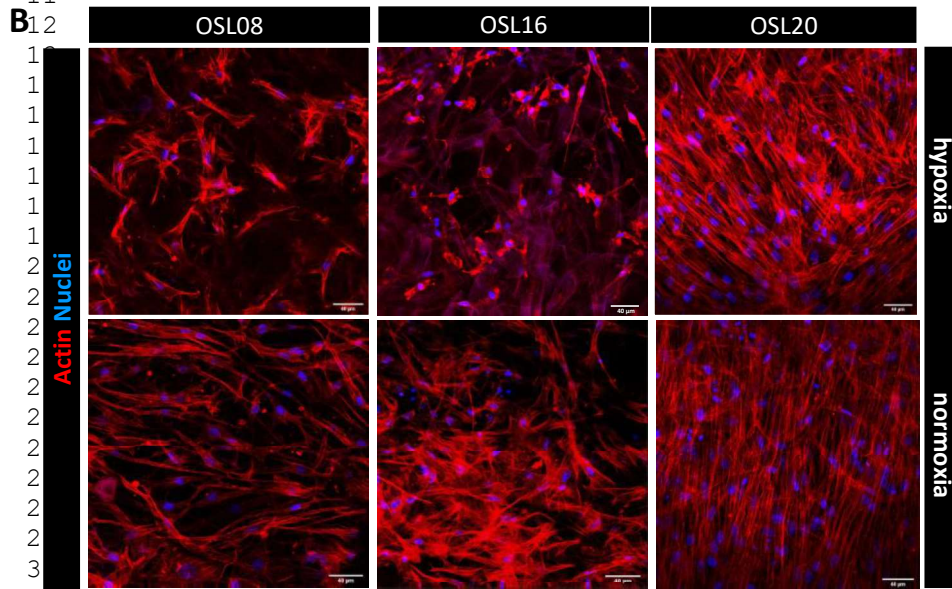
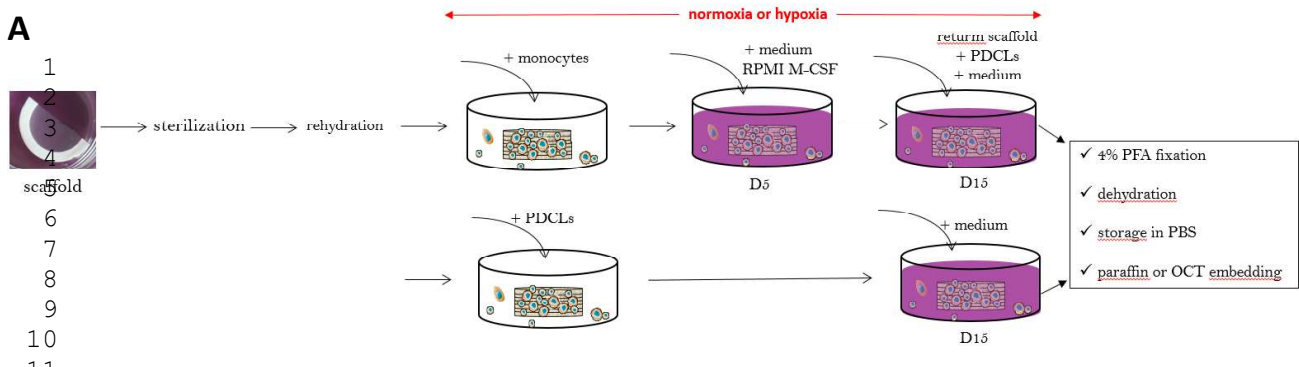
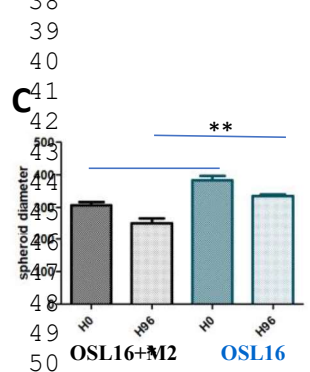
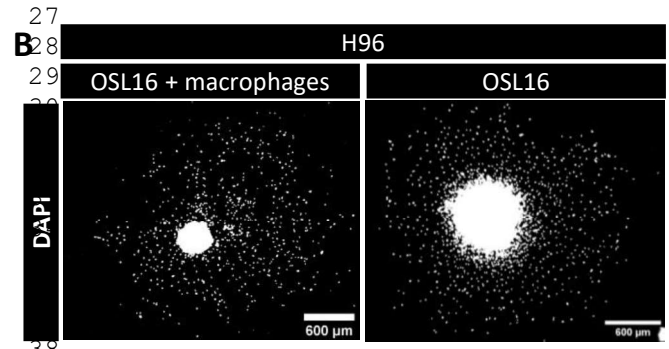
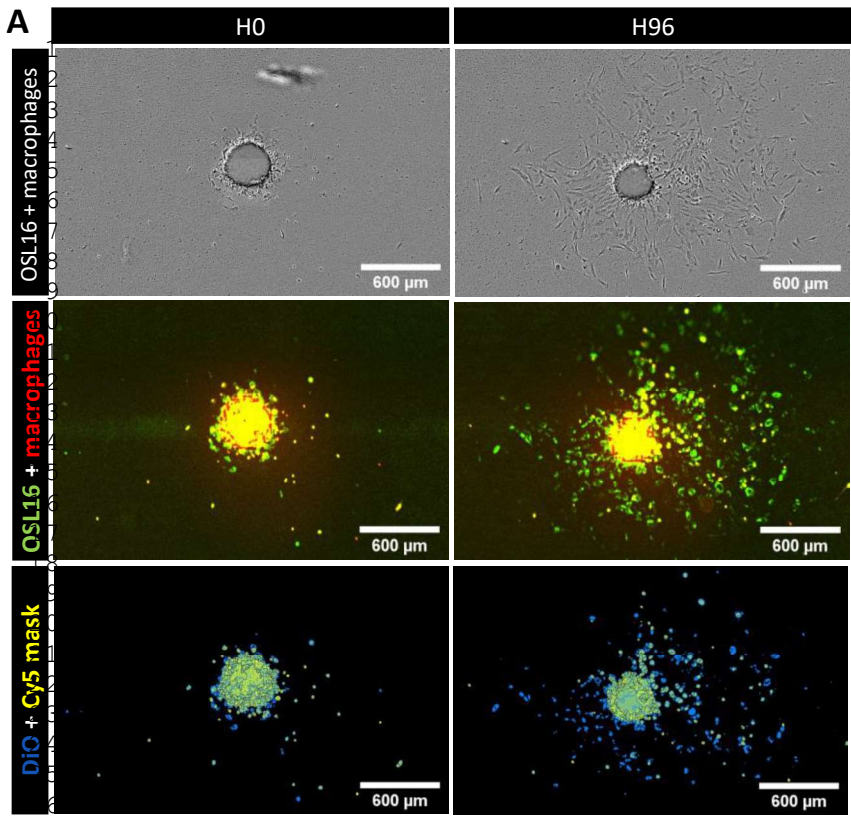


Figure 4: Bioengineering of extracellular microenvironment (bone scaffold and hypoxia) associating to immune and osteosarcoma cells



D

	OSL16 + macrophages				OSL16			
	H0		H96		H0		H96	
	Mean	SD	Mean	SD	Mean	SD	Mean	SD
Nb of evading cells	-	-	515	298.40	-	-	96.82	56.35
Spheroid diameter (μm)	306.98	17.81	253.10	26.07	384.97	20.87	333.60	10.02
Dist. mean (μm)	-	-	541.29	112.64	-	-	225.99	144.81

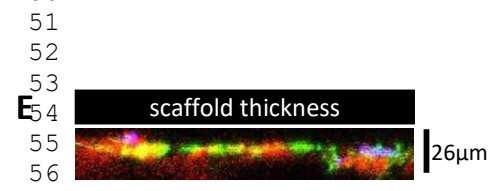
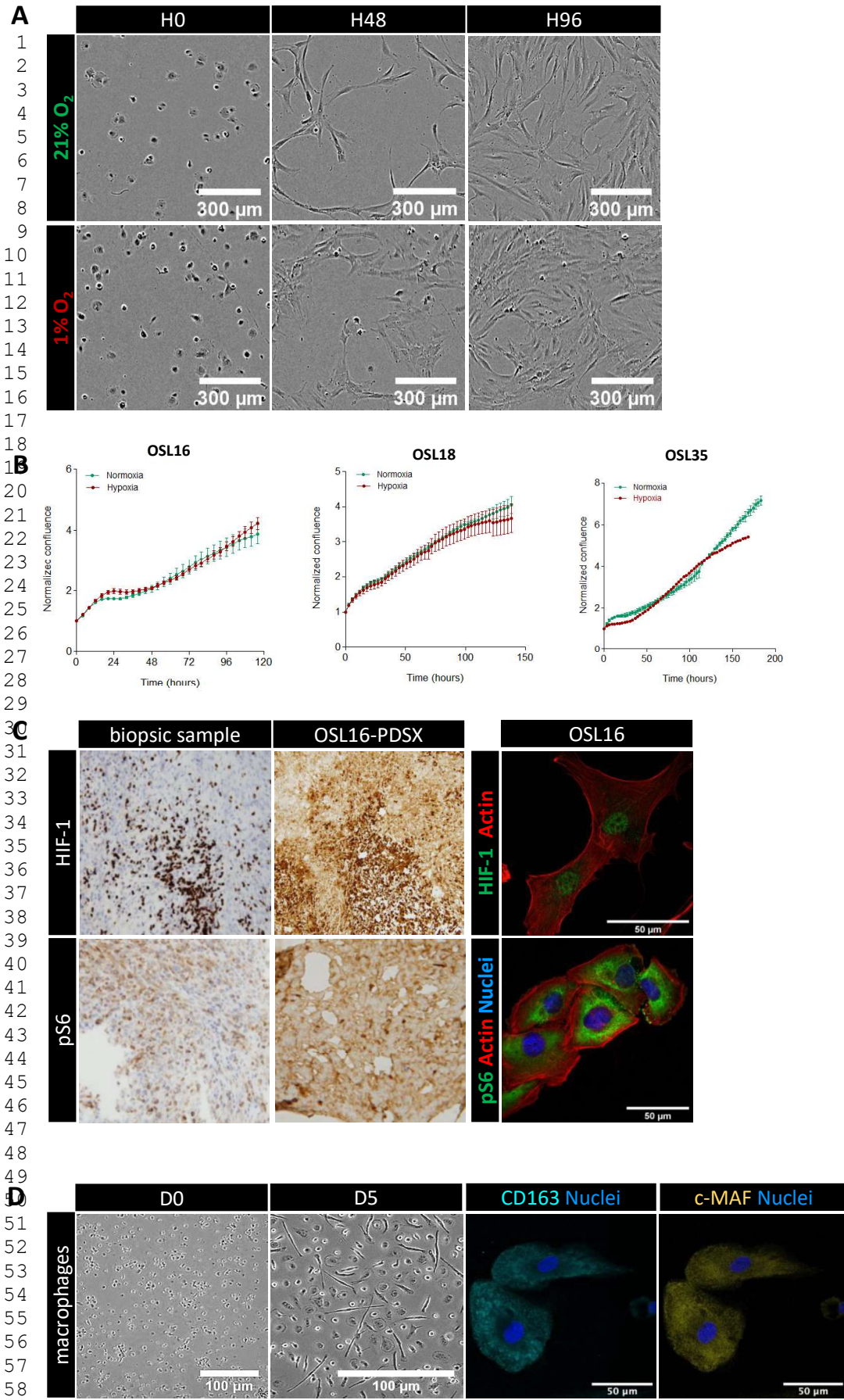
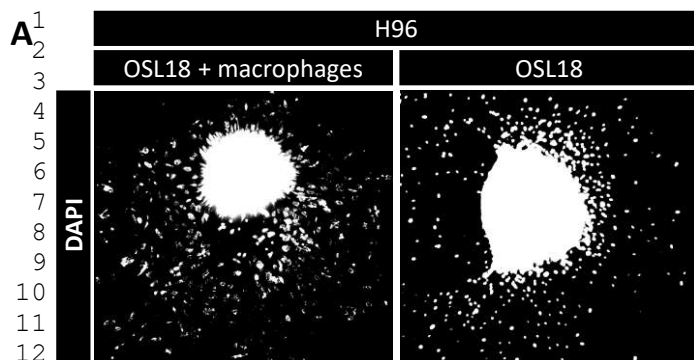


Figure 5: Migration assessment in 3D spheroid models and bone scaffold co-culturing M2 macrophages and osteosarcoma cells.



Supplemental Figure 1 : Extracellular and immune microenvironment engineering in 2D cultures of osteosarcoma PDCLs.

62
63
64
65



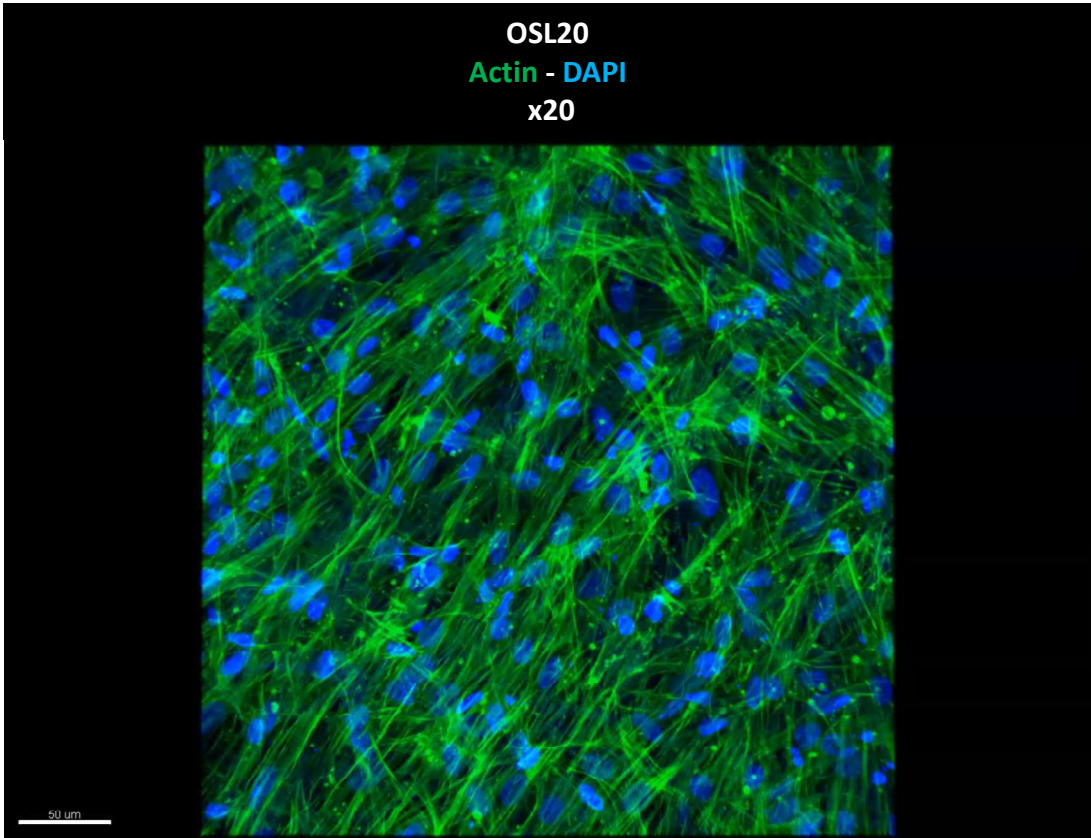
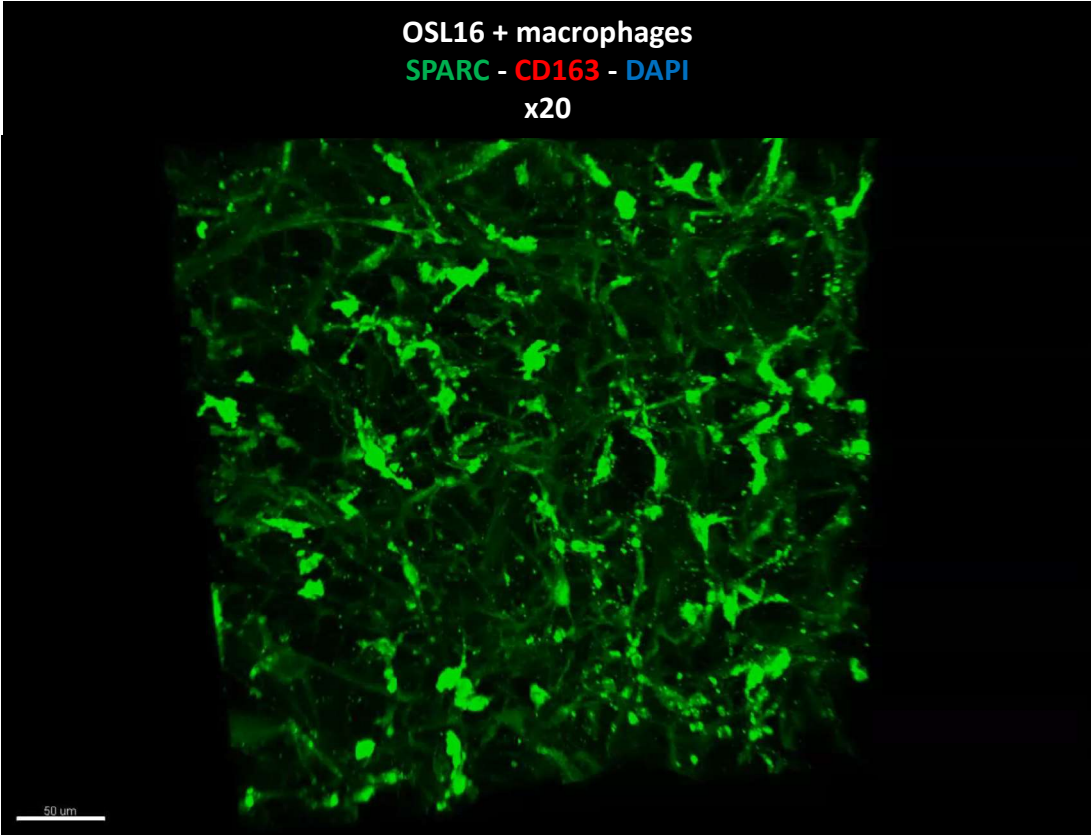
13
14
15
16
17
18
19
20
21
22
23
24
25

	OSL18 + macrophages				OSL18			
	H0		H96		H0		H96	
	Mean	SD	Mean	SD	Mean	SD	Mean	SD
Nb of evading cells	-	-	533	188.20	-	-	815.2	166.53
Spheroid diameter (μm)	574.07	38.1	529.56	54.5	650.24	62.66	576.5	40.15
Dist. mean (μm)	-	-	399.04	140.28	-	-	284.32	189.12

26
27
28
29 **Supplemental Figure 2 : Complementary data on migration assays in OSL18 line.**

30
31
32
33
34
35
36
37
38
39
40
41
42
43
44
45
46
47
48
49
50
51
52
53
54
55
56
57
58
59
60
61
62
63
64
65

1
2
3
4
5
6
7
8
9
10
11
12
13
14
15
16
17
18
19
20
21
22
23
24
25
26
27
28
29
30
31
32
33
34
35
36
37
38
39
40
41
42
43
44
45
46
47
48
49
50
51
52
53
54
55
56
57
58
59
60
61
62
63



Supplemental Figure 2: Videos obtained after reconstruction of the 3D-based scaffold culture's stacks with Imaris software. Immunofluorescent staining is as follows: nuclei are in blue (DAPI), SPARC and actin localized in osteosarcoma cells are in green and CD163+ macrophages are labeled in red.